MOLECULAR AND CELLULAR BIOLOGY, July 2002, p. 4914–4928 Vol. 22, No. 13
0270-7306/02/$04.00+0 DOI: 10.1128/MCB.22.13.4914–4928.2002

Yeast Ysl2p, Homologous to Sec7 Domain Guanine Nucleotide Exchange Factors, Functions in Endocytosis and Maintenance of Vacuole Integrity and Interacts with the Arf-Like Small GTPase Arl1p

Alexandra Jochum,[1] David Jackson,[2] Heinz Schwarz,[3] Rüdiger Pipkorn,[4] and Birgit Singer-Krüger[1]*

Institute for Biochemistry, University of Stuttgart, D-70569 Stuttgart,[1] Lion Bioscience[2] and Deutsches Krebsforschungszentrum,[4] D-69120 Heidelberg, and Max-Planck Institute for Developmental Biology, D-72076 Tübingen,[3] Germany

Received 17 January 2002/Returned for modification 14 February 2002/Accepted 9 April 2002

We previously described the isolation of *ysl2-1* due to its genetic interaction with Δ*ypt51*/*vps21*, a mutant with a deletion of the coding sequence for the yeast Rab5 homolog, which regulates endocytic traffic between early and late endosomes. Here we report that Ysl2p is a novel 186.8-kDa peripheral membrane protein homologous to members of the Sec7 family. We provide multiple genetic and biochemical evidence for an interaction between Ysl12p and the Arf-like protein Arl1p, consistent with a potential function as an Arf guanine nucleotide exchange factor (GEF). The temperature-sensitive alleles *ysl2-307* and *ysl2-316* are specifically defective in ligand-induced degradation of Ste2p and α-factor and exhibit vacuole fragmentation directly upon a shift to 37°C. In living cells, green fluorescent protein (GFP)-Ysl2p colocalizes with endocytic elements that accumulate FM4-64. The GFP-Ysl2p staining is sensitive to a mutation in *VPS27* resulting in the formation of an aberrant class E compartment, but it is not affected by a *sec7* mutation. Consistent with the idea that Ysl2p and Arl1p have closely related functions, Δ*arl1* cells are defective in endocytic transport and in vacuolar protein sorting.

Arfs constitute a ubiquitous subfamily of small GTPases in eukaryotes originally isolated as activators of cholera toxin-catalyzed ADP-ribosylation of purified Gαs (24) that are now known as critical and highly conserved components of diverse vesicular trafficking pathways and other cellular processes (34). The same Arf protein can regulate the formation of vesicles involved in a wide variety of transport steps. For example, the two yeast Arf family members Arf1 and Arf2, which are 96% identical and functionally interchangeable (51), function in transport through the endoplasmic reticulum (ER)-Golgi anterograde pathway and the Golgi-ER retrieval pathway and in reactions involving transport through the endosomal system (13, 29, 57).

Within the Arf family, the subgroup of the Arf-like (Arl) proteins has been defined based on sequence and functional relatedness (26). Arl proteins are structurally more divergent, with 40 to 60% sequence identity when aligned to any Arf protein or to each other. Arl proteins lack Arf activity, and, despite the fact that they contain a glycine at position 2, some (28, 45) but not all Arls may be subject to N myristylation, a modification that is essential for Arf function. Despite these variations, the structural resolution of human Arl3 and yeast Arl1p has provided evidence to place Arls into the Arf subfamily (2, 19). Functional overlap between Arf and Arl proteins was also revealed in a recent study (54). However, in contrast to the wealth of functional data on Arf proteins, very limited information on the role of Arl proteins in cellular physiology exists.

Small GTPases of the Rab/Ypt family constitute another large group of proteins with essential roles in membrane trafficking. These proteins are highly compartmentalized, making them excellent candidates for determining transport specificity and organelle identity (58). In the process of yeast endocytosis the homologues of mammalian Rab5, Ypt51p/Vps21p, Ypt52p, and Ypt53p have been implicated in the regulation of transport between early and late endosomes (41, 47, 48). Ypt51p/Vps21p has been shown to be independently involved in Golgi-to-endosome trafficking (14, 21).

Rab/Ypt and Arf proteins are inactive in the GDP-bound form. Activation, which requires replacement of bound GDP with GTP, is accelerated by guanine nucleotide exchange factors (GEFs), which serve as important regulators of Rab/Arf activity (34). While the GEFs for members of the Rab/Ypt family that have been identified generally have little similarity in primary sequence, several Arf GEFs that have homology with a domain of Sec7p have been identified (22). The so-called Sec7 domain, an approximately 200-amino-acid region, is, however, the only region of significant sequence similarity between Sec7p and other Arf GEFs. For most members the Sec7 domain alone is sufficient for guanine nucleotide exchange activity (4, 7, 23).

Here we report the sequence analysis and initial functional characterization of novel yeast protein Ysl2p, which represents a remote member of the Sec7 family of Arf GEFs. Ysl2p associates peripherally with endosomal elements and plays a role in endocytosis and the maintenance of vacuole structure. Genetic evidence and biochemical data suggest an interaction

* Corresponding author. Mailing address: Institut für Biochemie, Universität Stuttgart, Pfaffenwaldring 55, D-70569 Stuttgart, Germany. Phone: 049-711-685-4387. Fax: 049-711-685-4392. E-mail: Singer-Krueger@po.uni-stuttgart.de.

TABLE 1. Strains used

Yeast strain	Genotype	Source or reference
BS64	*MAT***a** *his4 ura3 leu2 lys2 bar1-1*	47
BS188	*MAT*α *his4 ura3 leu2 lys2 bar1-1*	49
RH732	*MAT***a** *his4 ura3 leu2 lys2 pep4*::*URA3 bar1-1*	H. Riezman, Basel, Switzerland
RH1201	*MAT***a**/α *his4/his4 ura3/ura3 leu2/leu2 lys2/lys2 bar1-1/bar1-1*	H. Riezman
BS694	*MAT***a** *his4 ura3 leu2 lys2 ysl2*::*kan*^{r} *bar1-1*	This study
BS747	*MAT***a**/α *his4/his4 ura3/ura3 leu2/leu2 lys2/lys2 ysl2*::*kan*^{r}/*ysl2*::*kan*^{r}*bar1-1/bar1-1*	This study
BS817	*MAT***a**/α *his4/his4 ura3/ura3 leu2/leu2 YSL2*::*GFP-kan*^{r}/*YSL2*::*GFP-kan*^{r} *sec7*/*sec7 bar1-1/bar1-1*	This study
BS819	*MAT***a**/α *his4/his4 ura3/ura3 leu2/leu2 YSL2*::*GFP-kan*^{r}/*YSL2*::*GFP-kan*^{r} *bar1-1*/*bar1-1*	This study
BS953	*MAT***a**/α *his4/his4 ura3/ura3 leu2/leu2 YSL2*::*GFP-kan*^{r}/*YSL2*::*GFP-kan*^{r} *vps27*/*vps27 bar1-1/bar1-1*	This study
BS1005	*MAT***a** *his4 ura3 leu2 lys2 arl1*::*kan*^{r} *bar1-1*	This study
BS1019	BS747 + pBS207	This study
BS1020	BS747 + pSF307	This study
BS1021	BS747 + pSF316	This study
BS1022	BS694 + pBS207	This study
BS1023	BS694 + pSF307	This study
BS1024	BS694 + pSF316	This study
BS1025	BS694 + pRS426-ARL1	This study
BS1103	*MAT***a** *his4 ura3 leu2 lys2 arl1*::*URA3 bar1-1*	This study
Y190	*MAT***a** *gal4 gal80 his3 trp1-901 ade2-101 ura3-52 leu2-3,112* + *URA3*::*GAL→lacZ LYS2*::*GAL→HIS3 cyh*^{r}	Steve Elledge, Houston, Tex.

between Ysl2p and the Arf-like small GTPase Arl1p. We reveal that Arl1p participates in endocytosis and vacuolar protein sorting. These results provide novel insights into the involvement of a new Sec7 family member and an Arl small GTPase in membrane trafficking within the endosomal system.

MATERIALS AND METHODS

Strains, media, and plasmids. Strains used in the study are listed in Table 1. Unless otherwise indicated, they were grown in complete medium (yeast extract-peptone-dextrose [YPD]) or synthetic dextrose (SD) growth medium to early logarithmic phase (0.5×10^7 to 2×10^7 cells/ml) at 25°C in a rotary shaker. To select for transformants carrying the *kan*^{r} marker, YPD plates containing 200 mg of G-418 sulfate (Calbiochem)/liter was used.

The plasmids used are listed in Table 2. All DNA manipulations were by standard techniques. *Escherichia coli* strain DH5α was used for cloning, and BL21(DH3) was used for expression of glutathione *S*-transferase (GST) fusion proteins.

Sequence analysis of Ysl2p. To assign putative functional domains within Ysl2p, neighborhood sequence analysis was performed. Homologues (producing an expectation value of less than 1e-14) to the query sequences, identified by searching the SWALL database (http://www.ebi.ac.uk/bic_sw/) were analyzed for their domain compositions. Once these were assessed, the ClustalW algorithm (52) was used to align Ysl2p against a multiple alignment of sequence fragments encompassing the domains identified in the homologues. Secondary structure prediction analysis was performed by using the PSI-PRED algorithm (32). All sequence identifiers were taken from entries of the SWALL database. The output residue groupings in Fig. 1 were taken from the CHROMA program (http://www.lg.ndirect.co.uk/chroma/index.htm).

Endocytosis of LY, FM4-64, Ste2p, and ^{35}S-α-factor. Lucifer yellow CH (LY) internalization experiments were performed with cells grown at 25°C as described previously (47). To determine the effect of a temperature shift to 37°C prior to LY internalization, strains were incubated at 37°C for 20 min prior to labeling with LY at 30°C for 1 h.

FM4-64 labeling was performed essentially as described previously (55) with, however, less FM4-64 (0.01 mM, final concentration). After incubation at 0°C for 30 min in SD medium, cells were washed, resuspended in SD medium prewarmed to 15°C, and incubated for 30 min at 15°C to accumulate the endocytic tracer in endosomal elements. Finally, cells were harvested, resuspended in fresh SD medium, and immediately viewed with a Zeiss Axiophot microscope equipped with appropriate Zeiss filters for green fluorescent protein (GFP) and FM4-64 fluorescence.

To monitor the pheromone-induced endocytosis of Ste2p, the method of reference 18 was used. Cells were removed after 0, 7.5, 15, 30, 60, and 120 min of incubation with α-factor at 30°C. Cell extracts were prepared and processed for immunoblotting with anti-Ste2p antiserum. Extracts of BS188 cells (*MAT*α), treated for 10 min with cycloheximide, served as a control for the specificity of the anti-Ste2p antiserum. Quantification of Ste2-specific bands was performed with a phosphorimager (Molecular Dynamics) and ^{125}I-protein A by immunoblot analysis.

Pheromone degradation assays were performed with biosynthetically labeled ^{35}S-α-factor using the pulse-chase protocol (10). The disappearance of intact and internalized α-factor was quantified as described before (10) with the help of the phosphorimager after an exposure time of 9 days.

Transmission electron microscopy. Yeast cells were cryoimmobilized by high-pressure freezing as described previously (20). In short, living cells were sucked into cellulose microcapillaries 200 μm in diameter and 2-mm-long capillary tube segments were transferred to aluminum platelets 200 μm deep containing 1-hexadecene. The platelets were sandwiched with platelets without any cavity and frozen with a high-pressure freezer (Bal-Tec HPM 010; Balzers). The frozen capillary tubes were freed from extraneous hexadecene under liquid nitrogen and transferred to microtubes containing the substitution medium precooled to −90°C. Samples were kept in 2% osmium tetroxide in anhydrous acetone at −90°C for 32 h, at −60°C for 4 h, and at −40°C for 8 h, at each step in a freeze substitution unit (FSU 010, Bal-Tec; Balzers). After being washed with acetone the samples were transferred into an acetone-Epon mixture at −40°C, infiltrated at room temperature in Epon, and polymerized at 60°C for 48 h. Ultrathin sections stained with aqueous uranyl acetate and lead citrate were viewed in a Philips CM10 electron microscope at 60 kV.

Invertase secretion. Cells grown at 25°C in YPD (5% glucose) were washed in yeast extract-peptone and resuspended in YPD (0.1% glucose) at 0.5 unit of optical density at 600 nm/ml to allow for the derepression of invertase. After a 30-min incubation at 30°C, cells were either left at 30°C or shifted to 37°C. Samples of 1 ml were removed after 0, 50, 60, and 70 min of incubation in YPD (0.1% glucose), transferred to 0°C, supplemented with NaN_3 (10 mM, final concentration), washed with ice-cold 10 mM NaN_3, and processed for the analysis of total and external invertase activity by the method of reference 15.

Pulse-chase labeling and immunoprecipitation of CPY. Pulse-chase labeling and immunoprecipitation of carboxypeptidase Y (CPY) were performed as described previously (49).

Generation of temperature-sensitive *ysl2* alleles by PCR mutagenesis. PCR mutagenesis was performed as described previously (36) with the 2.38-kb *Hpa*I/*Hpa*I fragment of the *YSL2* open reading frame (ORF) as the template and oligonucleotides 5′Sac-YSL2 (5′-TGGTGGATCCAAATATAC-3′) and 3′Pac-YSL2 (5′-TGATCAATTGTACTAATG-3′) annealing 228 bp upstream and 185

TABLE 2. List of plasmids

Plasmid	Characteristics	Source or reference
pBS207	*YSL2* in YCp50, isolated from genomic YCp50 library, includes coordinates 67948 to 78118 of chromosome XIV	This study
pBS313	*Nhe*I/*Sal*I fragment of *YSL2* in YEp24	This study
pBS337	*Nhe*I/*Sal*I fragment of *YSL2* in YIp5	This study
pSF307	Carries *ysl2-307*, derived from pBS207 by PCR mutagenesis	This study
pSF316	Carries *ysl2-316*, derived from pBS207 by PCR mutagenesis	This study
pFA6-kanMX4	Contains *kan*^{r}	56
pMK881	Same as pFA6a-GFP(S65T)-kanMX6	30
pRS426-ARL1	Contains *Bam*HI/*Xho*I fragment of *ARL1* including 446 bp 5′ of ATG and 136 bp 3′ of stop codon	This study
pRS426-ARL2	Contains *Bam*HI/*Xho*I fragment of *ARL2* including 485 bp 5′ of ATG and 204 bp 3′ of stop codon	This study
pRS426-ARL3	Contains *Bam*HI/*Xho*I fragment of *ARL3* including 492 bp 5′ of ATG and 291 bp 3′ of stop codon	This study
pFL-ARF1	*ARF1*, 2μm, *URA3*	Cathy Jackson, Bethesda, Md.
YEpARF2	*Sal*I/*Pst*I fragment of *ARF2* inserted into YEp352	Cathy Jackson
pBSK-Δarl1::URA3	*Cla*I/*Eco*RI fragment with *arl1*::*URA3* disruption cassette in pBSK-	This study
pACTII-18aaARL1^{T32N}	*Bam*HI/*Xho*I fragment of *ARL1*^{T32N} (encodes amino acids 19 to 183) in pACTII	This study
pACTII-18aaARL1^{G30A}	See pACTII-18aaARL1T32N, but G30A	This study
pACTII-18aaARL1^{Q72L}	See pACTII-18aaARL1T32N, but Q72L	This study
pGEM1-ARL1^{T32N}	*Hin*dIII/*Sal*I fragment of *ARL1*^{T32N} in pGEM1(*Hin*dIII/*Xho*I)	This study
pGEM1-18aaARL1^{T32N}	*Hin*dIII/*Sal*I fragment of −18aaARL1^{T32N} in pGEM1 (*Hin*dIII/*Xho*I)	This study
pAS1-Ysl2Sec7	*Bam*HI/*Sal*I fragment of *YSL2* (encodes amino acids 211 to 514) in pAS1	This study
pACTII-Ysl2Sec7	*Bam*HI/*Sal*I fragment of *YSL2* (as in pAS1-Ysl2Sec7) in pACTII(*Bam*HI/*Xho*I)	This study
pAS1-YPT51^{S21N}	*Bam*HI/*Sal*I fragment of *YPT51*^{S21N} in pAS1	This study
pGEX5-Ysl2Sec7	*Bam*HI/*Sal*I fragment of *YSL2* (as in pAS1-Ysl2Sec7) in pGEX5-3	This study
pGEX5-Ysl2Nterm	*Bam*HI/*Sal*I fragment of *YSL2* (encodes amino acids 2 to 514) in pGEX5-3	This study

bp downstream of the internal *Sac*I and *Pac*I restriction sites of *YSL2*, respectively. In the PCR, 4.8 mM $MgCl_2$, 0.2 to 0.4 mM $MnCl_2$, 0.2 mM dATP, 1 mM dCTP, 1 mM dGTP, and 1 mM dTTP were used. After purification of the PCR products using glass milk they were cotransformed with *Sac*I- and *Pac*I-digested pBS207 into strain BS747. Approximately 4,600 transformants were screened for growth at 25 and 37°C. Mutant plasmids were rescued from colonies that revealed growth at 25 but not 37°C and retransformed into BS747 to confirm the plasmid dependence of temperature-sensitive growth.

Generation of *YSL2* and *ARL1* gene disruptions. Large internal portions of genes *YSL2* and *ARL1* were deleted from the genome and replaced with the *kan*^{r} ORF of *E. coli*. For this, a simple PCR-based strategy was used to generate the kanMX module from plasmid pFA6-kanMX plus flanking regions of the genes to be disrupted (56). The generated PCR products were approximately 1,500 bp and were transformed into homozygous diploid strain RH1201, which was subjected to sporulation and dissection to obtain haploid deletion strains. Primers used were S1YSL2 (5′-CTCATCTCGCGATGGAGATTCAATTAAAAGTTTTACAGGTGGTACCCATTCGTACGCTGCAGGTCGAC-3′), S2YSL2 (5′-GCTATTCTATTTCTCAGGTTAGAACATGACATATAGCTGATTGCCTCAAATCGATGAATTCGAGCTCG-3′), S1ARL1 (5′-CTAAGAAGAAAGTTCCAGTAAAGTGAGTTATAGATCAAGATGGGTAACGTACGCTGCAGGTCGAC-3′), and S2ARL1 (5′-ATCTTTATCGCTATAACTGTTCCTCTTTTATAACATCAATCAACCAATCGATGAATTCGAGCTCG-3′).

A second *ARL1* disruption cassette containing *URA3* was generated. By PCR, the genomic flanking regions on either side of the *ARL1* ORF (−153 to 32 [5′FR] and 625 to 827 [3′FR]) were amplified from pRS426-ARL1. The PCR products were cloned into pBSK(-) by using *Cla*I and *Eco*RI restriction sites introduced by PCR. The resulting plasmid was opened with *Hin*dIII, and a 1.2-kb *URA3* fragment was ligated between the 5′FR and the 3′FR. Plasmid pBSK-Δarl1::URA3 was linearized with *Cla*I and *Eco*RI and used to transform BS64 in a one-step gene replacement. Ura$^+$ transformants were analyzed by PCR to verify the disruption of *ARL1*.

Construction of GFP-tagged Ysl2p. The chromosomal *YSL2*::*GFP* version was introduced with the help of the *kan*^{r} marker. A PCR-based strategy was used to generate the GFP-kanMX module from plasmid pFA6a-GFP(S65T)-kanMX6 (30). Oligonucleotides 5′GFP-YSL2 (5′-GATGGCCTCCAAGATAAAGTTTTGGAATTATCACTTGGATTTACGAAACTAGACCGTACGCTGCAGGTCGAC-3′) and 3′GFP-YSL2 (5′-CACACAACTATTTCTATAAGCATATCATACATACTACAATCTTATGTATATCGATGAATTCGAGCTCG-3′) contained at their ends additional 45-bp sequences homologous to the very 3′ end of the *YSL2* ORF (without a stop codon) and to a region 3′ of the *YSL2* stop codon. This allowed the targeted integration of the PCR products at the 3′ end of the *YSL2* locus. Upon transformation of the PCR products into diploid strain RH1201, transformants resistant to G-418 sulfate were purified and correct integration was verified by PCR. Subsequently, a heterozygous *YSL2*/*YSL2*::*GFP* strain was subjected to sporulation and tetrad dissection to obtain haploid epitope-tagged strains that grew indistinguishably from the wild type.

Generation of *arl1* mutants. DNAs encoding Arl1^{T32N}, Arl1^{G30A}, and Arl1^{Q72L} point mutants were generated by directed mutagenesis of *ARL1* DNA using a PCR-based protocol (3) and mutant primers 5′-GTAAACGATATAAGATGGTATTTTTACCTGCACCATCCAAACC-3′ (T32N), 5′-GTAAACGATATAAGATGGTAGTTTTAGCTGCACCATCCAAACCC-3′ (G30A), and 5′-GTAGGGCCTGATACTTGTCAAACCACCAAGATCCCAGAC-3′ (Q72L), respectively. As flanking primers 5′-TGGTGGATCCCAATGGGTAACATTTTTAGTTC-3′ and 5′-ACAGCTCGAGAAACATGTATACACT-3′ (3′ARL1,Xho) were used and pRS426-ARL1 was used as the template. The PCR products were digested with *Bam*HI and *Xho*I and subcloned into pACTII to generate pACTII-ARL1^{T32N}, pACTII-ARL1^{G30A}, and pACTII-ARL1^{Q72L}, respectively. PCR fragments encoding the N-terminal 18-amino-acid truncations of *arl1* mutants were generated with pACTII-ARL1^{T32N}, pACTII-ARL1^{G30A}, and pACTII-ARL1^{Q72L} as the DNA templates and primers 5′-TGGTGGATCCCATTGCGTATATTGATTTTGGG-3′ and 3′ARL1,*Xho*I. Subcloning the PCR fragments into pACTII was performed as described above. Two PCR fragments encoding ARL1^{T32N} and −18aaARL1^{T32N} were generated with primers 5′-TACCAAGCTTGTCAACATGGGTAACATTTTTAGTTC-3′ and 5′-TACCAAGCTTGTCAACATGTTGCGTATATTGATTTTGGG-3′, respectively, and 3′ARL1,*Xho*I and with pACTII-ARL1^{T32N} as the DNA template. After digestion with *Hin*dIII and *Xho*I, the PCR fragments were subcloned into pGEM1 (*Hin*dIII/*Sal*I) for in vitro transcription and translation from the SP6 promoter.

All PCR-amplified regions were sequenced to verify the mutations and to exclude the presence of PCR errors.

Generation of polyclonal antibodies against Ysl2p. A 2.5-mg sample of synthetic peptide representing an internal sequence of Ysl2p plus an additional N-terminal lysine (KRVHSFEELERHPDFA) was coupled to 4 mg of keyhole limpet hemocyanin as described previously (48). The immunization of rabbits was carried out by Eurogentec (Seraing, Belgium).

An affinity resin (Affi10-gel resin; Bio-Rad) to purify the anti-Ysl2p antiserum was prepared, and affinity purification of the anti-Ysl2p serum was performed as described previously (48). Concentration of the affinity-purified anti-Ysl2p antibody to 0.8 mg/ml was achieved by Centricon 10 filter devices.

Subcelluar fractionation by differential centrifugation and density gradient centrifugation. To monitor the distribution of Ysl2p and other marker proteins, subcellular fractionation of RH732 cells (*Δpep4*) was basically performed as described previously (46). For the preparation of spheroplasts, 1 mg of Zymolyase 100T/ml (final concentration) was used. After DEAE-dextran treatment, a precleared lysate devoid of unlysed cells was prepared by a spin at 300 × *g*. This was centrifuged at 3,500 × *g*, 13,000 × *g*, and 100,000 × *g* to obtain P1, P2, and P3, respectively. The supernatant of the spin at 100,000 × *g* corresponded to S3. Equal amounts of protein were separated by sodium dodecyl sulfate-polyacrylamide gel electrophoresis (SDS-PAGE) and subjected to immunoblotting with antibodies against Ysl2p, phosphoglycerate kinase, porin, alkaline phosphatase (ALP), Sec61p, Vps10p, Kex2p, and Ypt51p using ^{125}I-protein A as a detection system. Flotation analysis of the P3 fraction into a Nycodenz gradient was performed as described previously (48) using oxalyticase as the spheroplast enzyme (0.25 mg per 5 × 10^{10} cells). After centrifugation, 14 fractions were collected from the top of the gradient and equal volumes of each fraction were processed for immunoblotting. Quantitation of immunoreactive bands was performed with the phosphorimager.

Two-hybrid assays. Reporter strain Y190 was cotransformed with derivatives of pACTII (obtained from S. Elledge, Houston, Tex.) bearing wild-type and mutant forms of *ARL1* (see above) fused to the Gal4 transcriptional activation domain and pAS1-Ysl2Sec7 encoding the Sec7 domain of Ysl2p fused with the Gal4 DNA binding domain (constructed by subcloning a 0.9-kb *Bam*HI/*Sal*II fragment from pGEX5-Ysl2Sec7 into pAS1). As a control, Y190 was transformed with pAS1-YPT51^{S21N} (YPT51^{S21N} on a *Bam*HI/*Sal*I fragment was isolated from pGEM-Ypt51^{S21N} [48] and subcloned into pAS1) and pACTII-Ysl2Sec7 (constructed by subcloning a 0.9-kb *Bam*HI/*Sal*II fragment from pGEX5-Ysl2Sec7 into pACTII). Immunoblot analysis using a monoclonal antibody raised against the hemagglutinin epitope confirmed that cells expressed the corresponding fusion proteins. For quantitative assays, cells of four independent transformants were grown on SD-Ura-Trp-His–25 mM 3-amino-1,2,4-triazole plates for 4 days and the β-galactosidase activity was measured according to the *o*-nitrophenyl-β-D-galactopyranoside assay method described previously (16).

In vitro translation of *ARL1* alleles and in vitro binding studies with recombinant GST fusions. [^{35}S]methionine-labeled Arl1^{T32N}, and −18aaArl1^{T32N} were transcribed and translated in vitro with an SP6 polymerase TnT-coupled transcription-translation system from a rabbit reticulocyte lysate (Promega) according to the manufacturer's instructions. Arl1^{T32N} was synthesized in the presence of myristate (50 μM) bound to bovine serum albumin (6 μM). The quality of the preparations was analyzed by SDS-PAGE and autoradiography. The samples were quantified with the phosphorimager.

For GST pulldown experiments, two GST-Ysl2p fusion proteins were constructed by inserting PCR fragments encoding amino acids 2 to 514 (Ysl2Nterm, in pGEX5-Ysl2Nterm) or amino acids 211 to 514 (Ysl2Sec7, in pGEX5-Ysl2Sec7) into the bacterial expression vector pGEX5-3 (Pharmacia). All PCR-amplified regions were sequenced to exclude the presence of PCR errors. GST alone and GST fusions were expressed in BL21(DH3) cells after induction by addition of isopropyl-β-D-thiogalactopyranoside (1 mM, final concentration). After incubation for 3 h at 30°C, cells were harvested and stored at −20°C until used for purification. Both GST fusion proteins were soluble and purified under native conditions basically according to the manufacturer's instructions. Since the GST-Ysl2 fusions were unstable and partially degraded during the course of the purification, after elution from the affinity matrix with 5 mM glutathione–50 mM Tris-HCl, pH 8, the GST fusions were dialyzed for 2.5 h against 20 mM HEPES, pH 7.8-1 mM $MgCl_2$-1 mM dithiothreitol–0.2 mM phenylmethylsulfonyl fluoride with one buffer exchange. The dialysates were concentrated by Centricon 30 filter units (Millipore), and protein concentrations were determined by using the Bradford assay. Fractions containing purified GST and GST fusion proteins were stored in aliquots at −80°C.

For GST pulldowns, normalized (i.e., equimolar) amounts of in vitro-translated, ^{35}S-labeled proteins (Arl1^{T32N} and −18aaArl1^{T32N}) were incubated with glutathione-Sepharose beads complexed with GST (10 μg), GST-Ysl2Nterm (9.6, 19.2, or 38.4 μg), or GST-Ysl2Sec7 (30 μg) in 0.5 ml of buffer B (115 mM KCl, 5 mM NaCl, 20 mM HEPES [pH 7.8], 1 mM dithiothreitol, 2 mM $MgCl_2$, 0.05% NP-40, 100 μM GDP) for 3 h at 4°C. The beads were washed three times with 0.5 ml of buffer B. Bound proteins were eluted with SDS-PAGE sample buffer and subjected to SDS-PAGE, followed by autoradiography and Coomassie staining. Quantitation of ^{35}S-labeled proteins was performed with the phosphorimager.

RESULTS

Sequence analysis of Ysl2p. A novel mutant, *ysl2-1* (for *ypt51* synthetic lethal), was previously isolated; this allele displays synthetic lethality with the Δ*ypt51* strain, a strain with a deletion of a small GTPase that regulates transport between early and late endosomes (49). We cloned the corresponding wild-type gene by virtue of its ability to complement the temperature-sensitive growth of a *ysl2-1* strain at 37°C. This identified *YSL2*/*MON2* as ORF YNL297c (data not shown).

As deduced from the DNA sequence, Ysl2p is a protein with an apparent molecular mass of 186.8 kDa. Although initial analysis using transmembrane prediction algorithm TOPPREDII (9) suggested the existence of six potential transmembrane domains, analysis using more recent and accurate TMHMM and PHDhtm predictions (42, 50) did not support the idea of Ysl2p being a transmembrane protein (data not shown). Our biochemical data (see below) support this assertion.

Since initial sequence analysis using the heuristic BLAST algorithm or the HMMER profile-based search methods (1, 11) failed to assign putative functional domains within Ysl2p, we employed the so-called neighborhood analysis to provide this information. Clear homologues to the query sequence were analyzed for their domain compositions. The ClustalW algorithm was then used to align Ysl2p against a multiple alignment containing sequence fragments encompassing the domains of the homologous proteins. We noted a very clear bias in homology toward members of the Sec7 family. In each case, the homology was found N terminally, followed by the Sec7 domain. To test for the existence of an evolutionary remnant of the Sec7 domain within Ysl2p, we aligned it to a multiple sequence alignment of Sec7 domains using the ClustalW algorithm. Strikingly, a clear relationship was identified with this view (Fig. 1A; encompassing amino acids 221 to 504 of Ysl2p/YN37_YEAST). The reason why BLAST failed to detect this homology derives from the low sequence identity, coupled with the fact that the putative Ysl2p Sec7 domain contains a number of sequence insertions. Although larger, these insertions are still consistent with the occurrence of insertions in most of the other Sec7 domains (Fig. 1A) and may correspond to loop regions at the three-dimensional level.

To assess the secondary structural propensity of the putative Sec7 domain of Ysl2p, we also performed secondary structure prediction analysis using the PSI-PRED algorithm (32). In common with the crystal structure of the ARNO Sec7 domain (8, 35), the Ysl2p Sec7 domain was predicted to be all α-helical in nature. Moreover, the number of predicted α-helices was exactly consistent with the 10 found in the crystal structure of the ARNO Sec7 domain (data not shown). This finding highlights the fact that, while the sequence identity reflects a merely remotely homologous relationship to a typical Sec7 domain, the predicted underlying structural propensity is identical.

The homology to Sec7 family members was not restricted to the Sec7 domain. We also identified a novel highly conserved

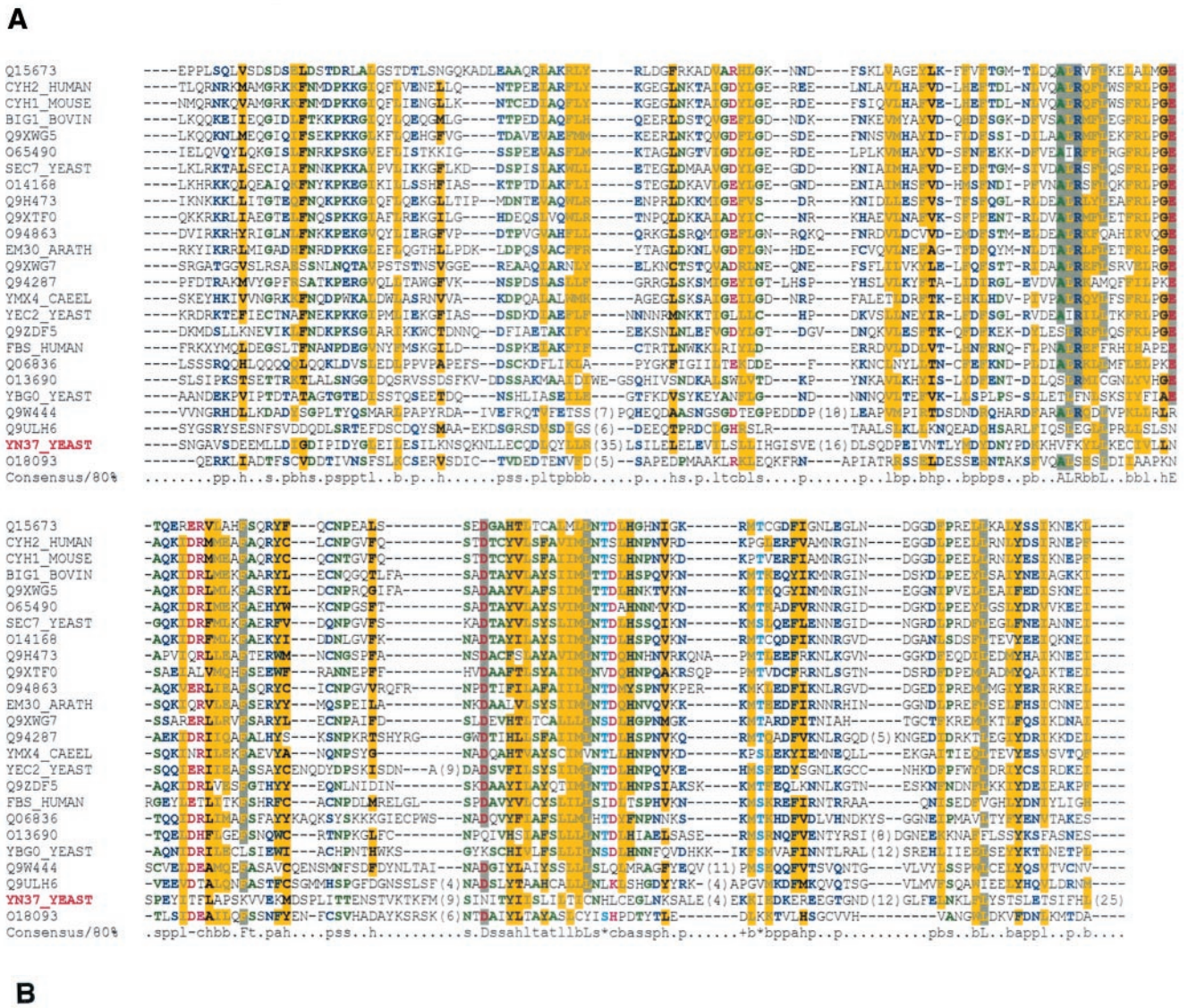

FIG. 1. *YSL2* encodes a novel protein with homology to Sec7 family GEFs. (A) Alignment of the putative Sec7 domain from Ysl2p/YN37_YEAST (identifier in boldface red) between positions 220 and 504 with 24 other Sec7 domains, as defined by the SMART database (44). (B) Alignment of the N-terminal region of Ysl2p/YN37_YEAST (amino acids 1 to 175) with five other Sec7 family members from mammals (Q9Y6D6/BIG1 and Q9Y6D5/BIG2), worms (Q19338 and Q9XWG5), and fission yeast (YAED_SCHPO). All sequence identifiers are taken from the SWALL database. Amino acid symbols are coded and shaded by property: yellow with gray shading, highly conserved; others are indicated in parentheses in the following consensus description. For the consensus sequence, the following symbols are used: +, positive (blue); −, negative (red); ∗, Ser/Thr (cyan); l, aliphatic (gray); t, tiny (green); a, aromatic (blue); c, charged (magenta); s, small (green); p, polar (blue); b, big (blue with light gray shading); h, hydrophobic (black with yellow shading); s, default.

N-terminal domain within Ysl2p (amino acids 1 to 175), which revealed the strongest homology and conservation in position and length when compared to the corresponding regions of several putative Sec7 family members of fission yeast (O14168, Q9UT02, and YAED_SCHPO), flies (Q9VLT1), and worms (Q19338 and Q9XWG5), which are at present poorly characterized. The alignment shown in Fig. 1B includes the well-characterized mammalian brefeldin A (BFA)-inhibited GEFs, such as BIG1 (Q9Y6D6) and BIG2 (Q9Y6D5) (31, 33, 53). In BIG1 and BIG2, the N-terminal region with homology to Ysl2p and the Sec7 domain are separated by approximately 480 amino acids.

Taken together, these in silico data provide substantial evidence for the existence of a remote Sec7 domain within Ysl2p and allow us to propose that Ysl2p may be a new member of the Sec7 family.

Ysl2p is required for endocytosis and maintenance of vacuole structure. To further explore the role of Ysl2p in endocytosis, we generated strains in which the ORF of *YSL2* was completely removed with the *kan*^{r} cassette. *YSL2*-deleted cells are viable but exhibit strong growth delays at all temperatures. At 37°C, Δ*ysl2* cells show hardly any growth (see Fig. 3A).

To monitor endocytosis, the pheromone-induced degradation of the α-factor receptor, Ste2p, was examined. After a short pretreatment with cycloheximide to inhibit new Ste2p synthesis, cells were harvested at various time points subsequent to the addition of α-factor. The degradation of internalized Ste2p was assessed by immunoblotting (Fig. 2A). In wild-type cells, before treatment with α-factor Ste2p migrates principally as a band of 45 to 47 kDa. Soon after the addition of pheromone a series of discrete high-molecular-mass bands are observed due to the hyperphosphorylation and ubiquitinylation of Ste2p (18) (Fig. 2A). Ste2p is then rapidly degraded as shown previously (43). Although Δ*ysl2* cells were not impaired in the kinetics of α-factor internalization at the plasma membrane (data not shown), they exhibited a strong delay in Ste2p turnover (Fig. 2A). While in the wild type the receptor was completely degraded 30 to 60 min after addition of α-factor, in Δ*ysl2* cells a large proportion of the initial 45- to 47-kDa band of Ste2p was still present after 120 min. Furthermore, the extent of modification leading to the high-molecular-mass forms of Ste2p was reduced compared to that for the wild type. We also analyzed the fate of internalized α-factor. Similar to the original *ysl2-1* mutant (49), Δ*ysl2* cells were clearly delayed in the degradation of the internalized pheromone (see Fig. 8D).

Unlike wild-type vacuoles, which appeared as large structures accumulating endocytic fluid phase marker LY after a 60-min incubation at 30°C, vacuoles of Δ*ysl2* cells were highly fragmented (Fig. 2B; see also below). The granular structures were only weakly labeled by LY, most likely due to the reduced rate of endocytosis.

Conditional *YSL2* mutants were generated to define more precisely the direct function of Ysl2p. For this, the sequence of *YSL2* that encodes amino acids 1040 to 1494 was subjected to PCR-mediated random mutagenesis, leading to the isolation of mutants that grew markedly better than the Δ*ysl2* mutant at the permissive temperature of 25°C but that were reversibly temperature sensitive at 37°C (Fig. 3A).

To analyze the effect of a temperature shift on fluid phase endocytosis and vacuole morphology, two novel temperature-sensitive alleles, *ysl2-307* and *ysl2-316*, were characterized. Upon internalization with LY at 30°C for 1 h, both mutants exhibited LY-labeled vacuoles similar to those of the wild type (Fig. 3B, *ysl2-316* not shown). In contrast, a 20-min preshift to 37°C before the 1-h incubation with LY at 30°C resulted in rapid fragmentation of the vacuole (Fig. 3B). Importantly, the morphology of wild-type vacuoles was not affected by the preshift to 37°C (Fig. 3B). Longer preincubations of mutant cells at 37°C resulted in a more pronounced fragmentation of the vacuole (data not shown) reminiscent of that shown by Δ*ysl2* cells (Fig. 2B).

To confirm the dramatic change in vacuolar morphology at the ultrastructural level, wild-type, Δ*ysl2*, and *ysl2-316* cells were quick-frozen after growth at 25°C or after a shift to 37°C and subsequently analyzed in the electron microscope. Wild-type and *ysl2-316* cells grown at 25°C usually contained few (one to three) large vacuoles per central section (Fig. 3C), which were clearly distinguishable from the nucleus by their

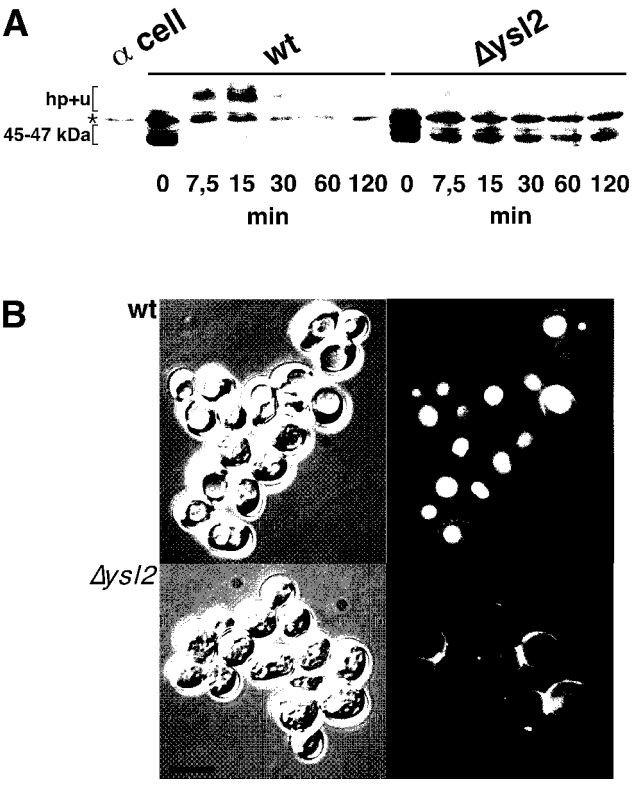

FIG. 2. The Δ*ysl2* mutant is blocked in the degradation of Ste2p and contains highly fragmented vacuoles. (A) Pheromone-stimulated internalization of Ste2p was analyzed on cells (BS64 and BS694) grown at 25°C. After a 10-min preincubation in the presence of 10 μg of cycloheximide/ml, α-factor was added and, at the indicated times, samples were withdrawn and processed for immunoblotting with an anti-Ste2p antiserum. A cell extract of α-mating-type cells lacking Ste2p is shown (α cell, BS188) to reveal a band (*) unspecifically labeled by the anti-Ste2p serum. The positions of the 45- to 47-kDa and lower-mobility forms of Ste2p (hp+u) are indicated. wt, wild type. (B) LY internalization assays were performed with cells (RH1201 and BS747) grown at 25°C. After a 1-h incubation with LY at 30°C, the cells were washed, mounted in low-melting-point agarose, and visualized by using fluorescence (right) and Nomarski optics (left). Bar, 10 μm.

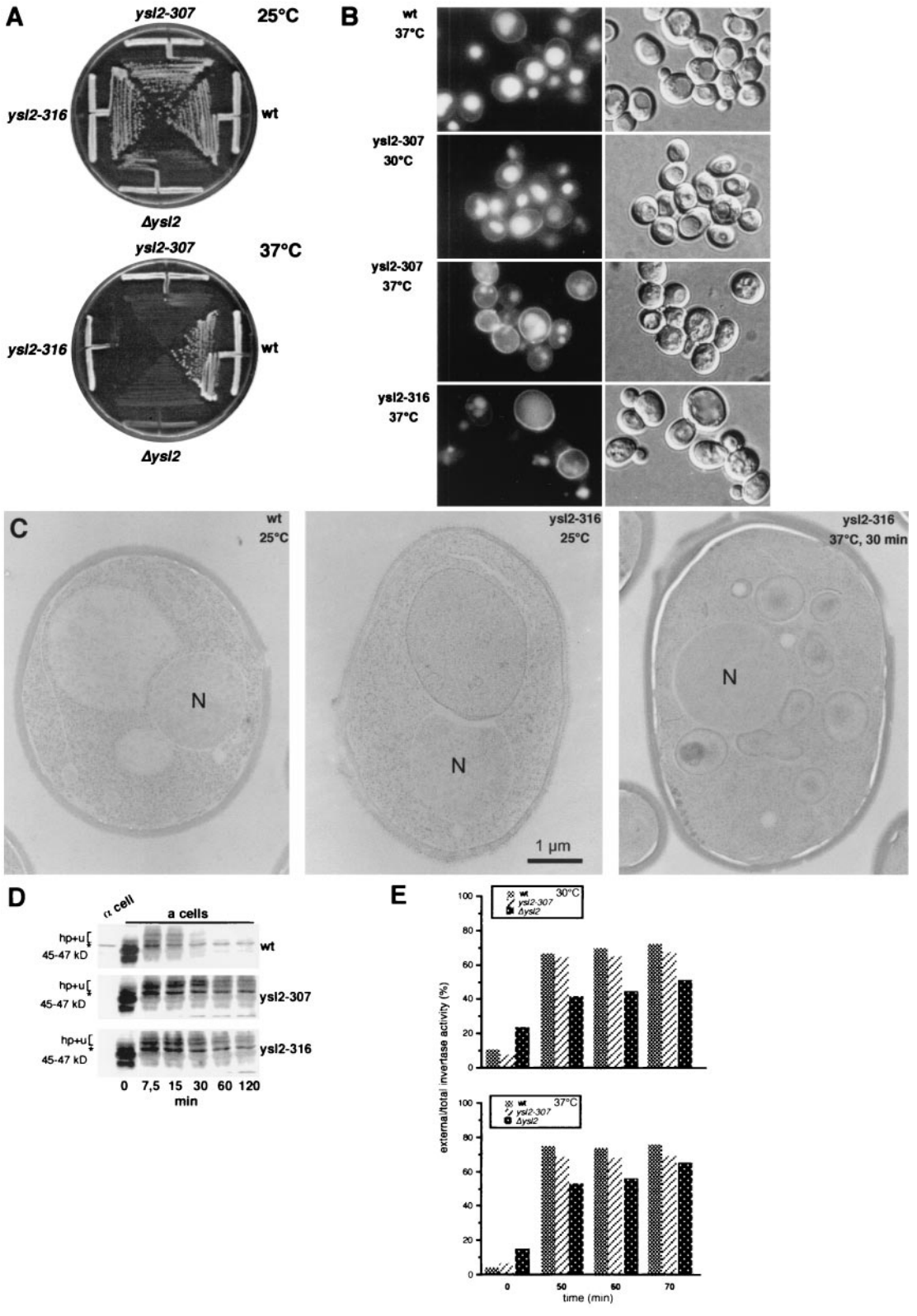

FIG. 3. The temperature-sensitive *ysl2-307* and *ysl2-316* mutants exhibit vacuole fragmentation rapidly upon a shift to the nonpermissive temperature and are specifically defective in the degradation of Ste2p at the permissive temperature. (A) Growth of wild-type (wt; BS1019) cells, strains carrying temperature-sensitive alleles *ysl2-307* (BS1020) and *ysl2-316* (BS1021), and the Δ*ysl2* strain (BS747 carrying the empty YCp50 vector). Cells were streaked out on YPD and incubated at 25 and 37°C. (B) LY internalization assays either were directly performed at 30°C with cells described in the panel A legend or were performed with cells that were incubated at 37°C for 20 min prior to the 1-h incubation with LY at 30°C. After being washed, cells were visualized by using fluorescence (left) and Nomarski optics (right). Bar, 10 μm. (C) RH1201 (wild type) and

different matrix density. In contrast, *ysl2-316* cells quick-frozen after a 30-min shift to 37°C were characterized by an immediate fragmentation of the vacuolar compartment (Fig. 3C). Similarly, Δ*ysl2* cells and *ysl2-316* cells shifted to 37°C for 2 h exhibited a severe vacuolar breakdown (data not shown). Thus, the data obtained by light and electron microscopy clearly demonstrate that vacuole fragmentation was an immediate, and therefore most likely a direct, consequence of heat inactivation of Ysl2p.

Since endocytosis is not essential for life, many endocytosis mutants reveal transport defects even at their permissive growth temperature. Therefore, it was not surprising that *ysl2-307* and *ysl2-316* cells were strongly delayed in α-factor-induced Ste2p degradation when grown at 25°C and treated at 30°C during receptor internalization (Fig. 3D). In contrast to Δ*ysl2* cells (Fig. 2B), in which primarily the 45- to 47-kDa form of Ste2p was stabilized, *ysl2-307* and *ysl2-316* cells accumulated both the 45- to 47-kDa and the hyperphosphorylated and ubiquitinylated forms, suggesting that the transport block may not be as tight as in Δ*ysl2* cells. This notion was supported by the fact that the rate of degradation of internalized α-factor was slightly less delayed in the *ysl2* temperature-sensitive mutants than in Δ*ysl2* cells (see Fig. 8D). Since at 30°C *ysl2-307* and *ysl2-316* cells did not reveal other transport defects (see below), these findings strongly suggest that Ysl2p plays a direct role in endocytosis.

Secretion of invertase and vacuolar sorting of CPY are largely unaffected in conditional *ysl2* mutants at the permissive temperature. In the newly generated *ysl2* mutants (Δ*ysl2*, *ysl2-307*, and *ysl2-316* mutants) the kinetics of CPY biogenesis were comparable to those in wild-type cells (data not shown). However, as observed for the *ysl2-1* mutant (49), all other *ysl2* mutants analyzed exhibited a slight missorting of p2CPY to the extracellular space at the permissive and nonpermissive temperatures. However, compared to what was found for Δ*ysl2* cells, in *ysl2-307* and *ysl2-316* cells the fraction of total CPY that was missorted as the p2 form was smaller (7.5% in *ysl2-307* cells and 4% in *ysl2-316* cells versus 15% in Δ*ysl2* cells). The small magnitude of CPY missorting displayed by all *ysl2* mutants, even the barely viable Δ*ysl2* strain, argues against the idea that Ysl2p plays a direct role in CPY sorting.

We also examined the secretion of invertase in the different *ysl2* mutants. After the derepression of invertase by incubation in 0.1% glucose at 30 or 37°C, *ysl2-307* cells exhibited a ratio of external to total invertase that was similar to (30°C) or only slightly reduced from (37°C) that for the wild type (Fig. 3E). In contrast, Δ*ysl2* cells exhibited a ratio of secreted invertase to total invertase that was reduced at all temperatures tested. In addition, the kinetics of invertase secretion were clearly delayed. Thus, while *ysl2-307* cells exhibit no defect in the transport of invertase, transport is impaired in Δ*ysl2* cells.

Ysl2p is highly enriched in a membrane fraction produced by centrifugation at 100,000 × *g* that cofractionates with endosomal membranes. To characterize the *YSL2* gene product and its subcellular localization, we raised an antipeptide antiserum which specifically recognized a polypeptide present in a crude cell extract of the wild type whose size corresponds to the expected size of Ysl2p (186.8 kDa) (data not shown).

To determine the subcellular fraction in which Ysl2p is enriched, differential centrifugation of a precleared lysate was performed at 3,500 × *g* (P1), 13,000 × *g* (P2), and 100,000 × *g* (P3). The presence of Ysl2p and other marker proteins in pellet fractions P1 to P3 and the supernatant of the spin at 100,000 × *g* (S3) was determined by immunoblotting (Fig. 4A). The sedimentation profile of Ysl2p did not resemble that of vacuolar marker ALP or that of the mitochondrial protein porin. It was also clearly distinct from the sedimentation profile of Sec61p, an ER marker protein. In contrast, Ysl2p was mostly enriched in pellet fraction P3. This fraction mainly contains small organelles such as Golgi elements (Vps10p) and endosomes. Therefore, from differential centrifugation, it could be presumed that a major fraction of Ysl2p is likely associated with Golgi elements and/or endosomes. Although it is not obvious in the experiment shown in Fig. 4A, other experiments have shown that a fraction of Ysl2p is also present in the cytosol.

Density gradient centrifugation of the P3 fraction revealed that Ysl2p floated with membranes (Fig. 4B). In the gradient, it fractionated most similarly to endosomal membranes containing the small GTPase Ypt51p/Vps21p (48) (Fig. 4B) and Pep12p (not shown). A partial cofractionation was also found with trans-Golgi marker proteins Vps10p and Kex2p (Fig. 4B). Again, these data are consistent with an association of Ysl2p with endosomes and/or the late Golgi compartment.

To analyze the nature of association of Ysl2p with membranes, the P3 fraction was treated on ice with various reagents. While treatment with 8 M urea, 1 M NaCl, or 0.1 M $NaCO_3$, pH 11, resulted in a partial release of Ysl2p into the supernatant, Ysl2p was not extracted from the pelletable fraction upon incubation with various detergents (data not shown). These results suggest that Ysl2p is not an integral membrane protein but rather associates with membranes peripherally.

GFP-Ysl2p colocalizes with endocytic elements labeled by FM4-64. To directly observe Ysl2p localization in living cells, the protein was epitope tagged with the GFP at its C terminus. This was accomplished by the integration of a PCR product via homologous recombination into the 3′ region of the authentic *YSL2* locus yielding a *GFP* fusion gene transcribed from the endogenous promoter. Epitope-tagged GFP-Ysl2p was fully functional as the only copy of Ysl2p (see Materials and Methods). Microscopic analysis of diploid cells homozygous for *YSL2*::*GFP* revealed a punctate staining pattern showing on

BS1021 (*ysl2-316*) were grown in YPD at 25°C to early log phase. Cells were either directly cryoimmobilized and processed for electron microscopy (EM) as described in Materials and Methods or shifted to 37°C for 30 min, quick-frozen, and processed for EM analysis. Thin sections were viewed in the electron microscope. N, nucleus. (D) α-Factor-induced internalization of Ste2p was analyzed on cells (BS1022, BS1023, and BS1024) at 30°C as described for Fig. 2A. ∗, band specifically labeled by the anti-Ste2p serum. (E) Invertase secretion was performed with cells listed in the panel D legend, which were grown in YPD (5% glucose) at 25°C. Invertase derepression was induced in YPD (0.1% glucose) at 30°C for 30 min. Subsequently the cells were either left at 30°C or shifted to 37°C. Samples were analyzed for external and total invertase activity after 0-, 50-, 60-, and 70-min periods of invertase derepression. The values represent means of three different experiments.

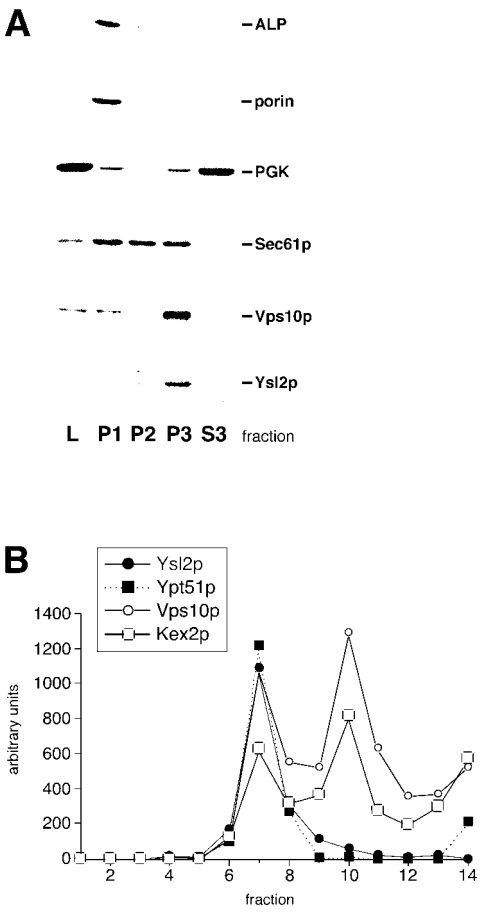

FIG. 4. Ysl2p is highly enriched in a membrane pellet fraction produced by centrifugation at 100,000 × *g* and cofractionates with endosomal membranes upon flotation into a Nycodenz gradient. (A) Wild-type cells (RH732) were converted to spheroplasts and lysed with DEAE-dextran. The precleared lysate was subjected to differential centrifugation at 3,500 × *g*, 13,000 × *g*, and 100,000 × *g* to generate pellet fractions P1, P2, and P3 and supernatant fraction S3. Immunoblot analysis was performed with antibodies against Ysl2p and marker proteins for ALP (vacuole), porin (mitochondria), phosphoglycerate kinase (cytosol), Sec61p (ER), and Vps10p (late Golgi). (B) The P3 fraction pellet was resuspended in 37% Nycodenz, overlaid with different solutions of Nycodenz, and subjected to equilibrium density gradient centrifugation. Fourteen fractions were collected from the top of the gradient, and equal volumes per fraction were analyzed by immunoblotting with antibodies against Ysl2p, Ypt51p, Vps10p, and Kex2p using ^{125}I-protein A as a detection system. The bands were quantified with the phosphorimager (Molecular Dynamics).

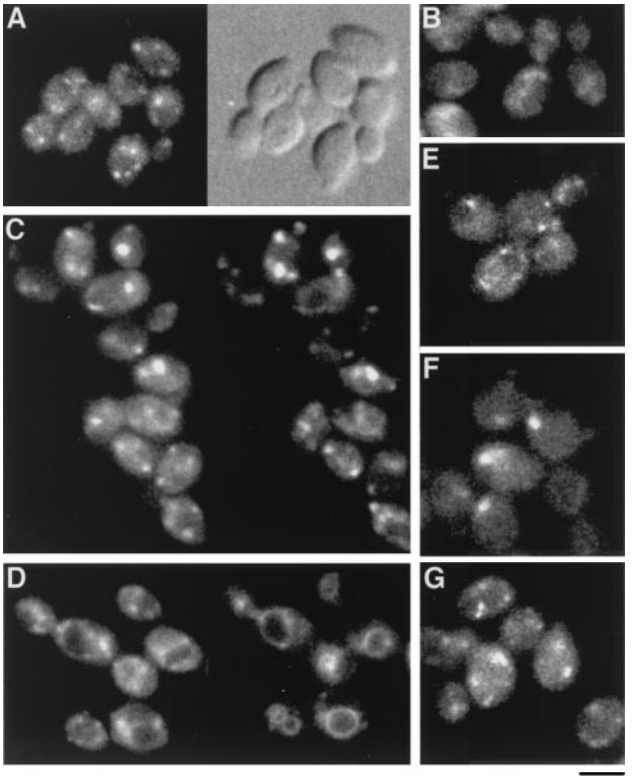

FIG. 5. GFP-Ysl2p is localized to punctate structures. (A and B) BS819 (homozygous diploid for *YSL2*::*GFP*) (A) and RH1201 (B) cells were processed for fluorescence microscopy as described in Materials and Methods. Images were obtained by fluorescence (left) and Nomarski optics (right). Bar (applies to all panels), 10 μm. (C) After BS819 cells were labeled with FM4-64 for 30 min at 0°C, cells were resuspended in SD prewarmed to 15°C to allow the accumulation of FM4-64 during a 30-min incubation. Subsequently, cells were collected, resuspended in fresh medium, and photographed within 2 min with appropriate filters for GFP (left) and FM4-64 (right) fluorescence. (D) BS819 cells were incubated with FM4-64 as described for panel C with the difference that FM4-64 was internalized at 30°C for 30 min to allow transport of FM4-64 to the vacuole. (E to G) BS819 (wild type; E), BS953 (*vps27*; F), and BS817 (*sec7*; G) cells were grown at 25°C. BS819 and BS953 cells were directly used to analyze the pattern of GFP-Ysl2p fluorescence as described for panel A. BS817 (*sec7*) cells were harvested, resuspended in YP medium prewarmed to 37°C containing 0.1% glucose, and incubated at 37°C for 2 h to induce the Golgi defect caused by mutant *sec7*. Subsequently, cells were viewed as described for panel A.

average between four and six Ysl2p-positive dots per cell (Fig. 5A and E) that were not visible in cells of an untagged strain (Fig. 5B). The Ysl2-GFP staining was, however, quite weak. This suggests that Ysl2p is a protein of low abundance, as indicated by its rare codon usage, or that only a fraction of Ysl2p is membrane associated. The dot-like staining is typical both for endosomes and Golgi elements. To determine whether the Ysl2p-positive structures were endocytic in nature, several approaches were chosen. First, we investigated whether GFP-Ysl2p colocalized with FM4-64, a fluorescent styryl dye which is transported along the endocytic pathway and whose excitation-emission spectrum is compatible with GFP for double-fluorescence studies. After binding at 0°C, FM4-64 was internalized at 15°C to cause its accumulation in early and late endosomes, which appear as punctate structures distributed throughout the cell (55). As shown in Fig. 5C, FM4-64 fluorescence obtained after internalization at 15°C colocalized in several cases with GFP-Ysl2p fluorescence. This colocalization was not observed when FM4-64 was internalized at 30°C for 30 min and therefore delivered to the vacuole (Fig. 5D).

As a second test we took advantage of the observation that in *vps* class E mutants, such as *vps27*, the prevacuolar compartment forms the aberrant endosomal class E compartment, which appears as a single, abnormally enlarged structure in proximity to the vacuole (40). If the Ysl2-GFP fusion protein resides on endosomal elements, the punctate structures should

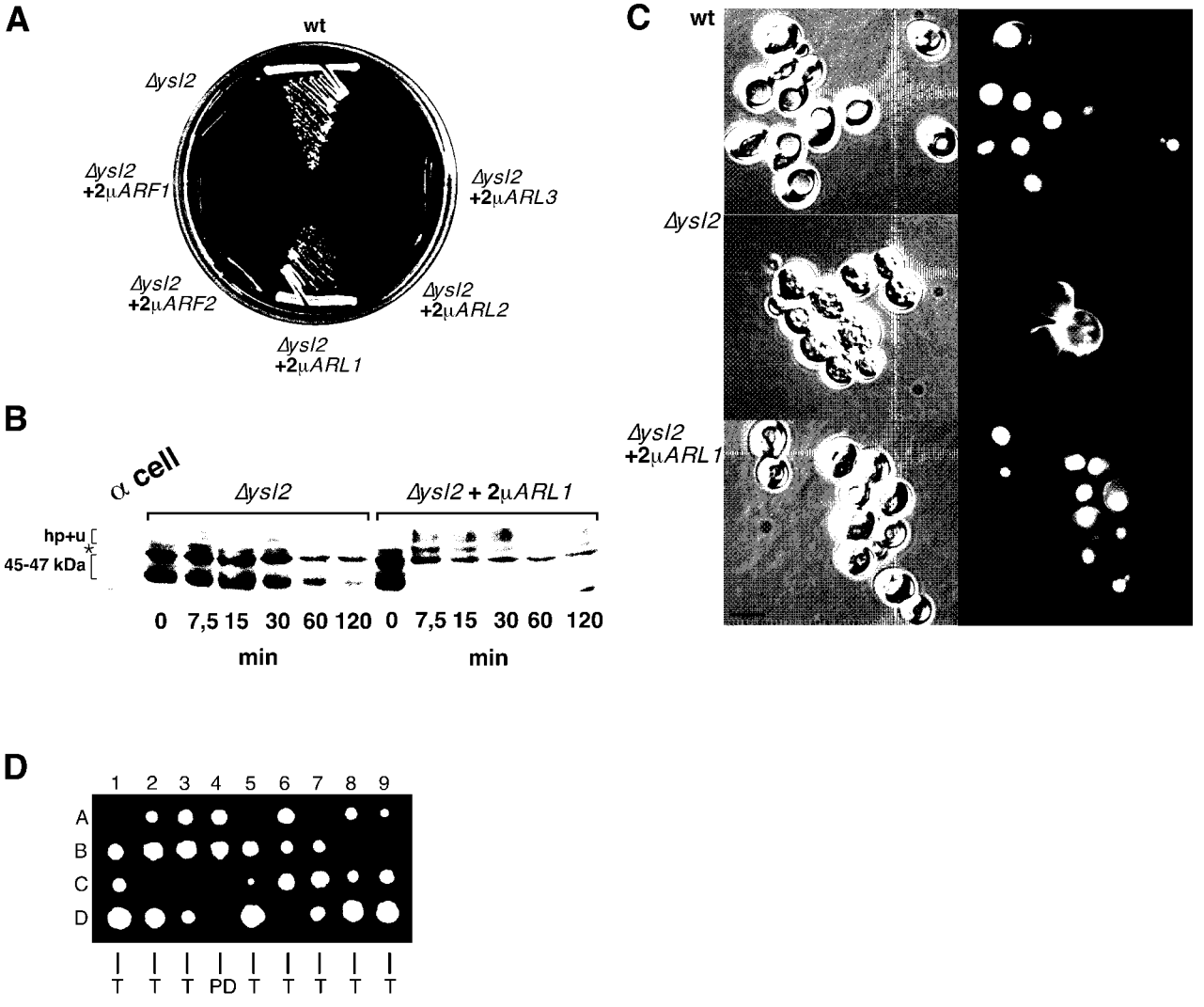

FIG. 6. *ARL1* reveals multiple genetic interactions with *YSL2*. (A) Δ*ysl2* (BS747) cells were transformed with 2μm plasmids containing either *ARF1*, *ARF2*, *ARL1*, *ARL2*, or *ARL3*. Ura$^+$ transformants were streaked out on YPD and incubated at 37°C. wt, wild type. (B) Pheromone-stimulated internalization of Ste2p was analyzed in BS694 *(*Δ*ysl2*) cells transformed with either 2μm-*ARL1* or vector alone as described for Fig. 2A. *, band specifically labeled by the anti-Ste2p serum. (C) LY internalization was analyzed in BS747 (Δ*ysl2*) cells, BS747 cells transformed with *CEN*-based *YSL2* (wild type), and BS747 cells transformed with 2μm-*ARL1* as described for Fig. 2B. Cells were visualized by using fluorescence (right) and Nomarski optics (left). Bar, 10 μm. (D) Δ*ysl2* and Δ*arl1* mutations are synthetic lethal. Δ*ysl2* cells (BS695; *kan*^{r}) were crossed with Δ*arl1* cells (BS1103; Ura$^+$). Following sporulation and tetrad dissection (47 tetrads, in total), colonies were grown at 25°C. Shown are nine tetrads (1 to 9, each A to D) that were tetratype (T) or nonparental ditype (NPD), based on auxotrophy and resistance to G-418. In all cases, the haploid progeny predicted to be G-418 resistant and Ura$^+$ failed to grow at 25°C.

become larger and less numerous in the *vps27* mutant. As shown (Fig. 5F), a clear change of GFP-Ysl2p labeling was indeed observed in *vps27* cells. The multiple Ysl2p-positive spots collapsed into a single, larger structure reminiscent of the class E compartment. Finally, it has been found that a mutation in *SEC7* results in the formation of Golgi stacks, with the effect that the fluorescence pattern of Golgi markers becomes larger and less numerous in *sec7*-shifted cells (37). Upon a 2-h incubation at 37°C in medium containing a low glucose concentration, the fluorescence pattern of Ysl2p-GFP was unaffected in *sec7* cells (Fig. 5G) and resembled that of the wild type. The distinct effects of mutations, together with the finding that GFP-Ysl2p staining colocalized with endocytosed FM4-64 after internalization at 15°C, strongly supports the idea that GFP-Ysl2p is localized to an endocytic compartment(s) that is accessed by endocytosed material at 15°C and that is sensitive to mutations in class E *VPS* genes.

Ysl2p reveals genetic interactions with the Arf-like small GTPase Arl1p. To identify proteins that function together with Ysl2p or that bypass the requirement for Ysl2p, a screen for high-copy-number suppressors in cells carrying the *ysl2-307* allele was performed. This led to the isolation of clones containing a fragment of chromosome II including the *ARL1* gene. This gene was amplified by PCR, and upon subcloning into a 2μm-based vector it was transformed into *ysl2-307* and Δ*ysl2* cells. This demonstrated that *ARL1* is a high-copy-number

suppressor of Δ*ysl2* and *ysl2-307* cells (not shown) at 37°C (Fig. 6A). *ARL1* encodes a member of the Arf family of small GTPases. In yeast four other members of this family exist. Although none of them was identified as a suppressor of *ysl2*, except *ARL1*, Δ*ysl2* cells were transformed with 2μm plasmids carrying *ARF1*, *ARF2*, *ARL2*, or *ARL3* and the ability of each gene to suppress the growth defect of Δ*ysl2* cells was compared to that of *ARL1*. As depicted in Fig. 6A, suppression of Δ*ysl2* cells was exclusively caused by the overexpression of *ARL1* and therefore was highly specific.

Overexpression of *ARL1* in Δ*ysl2* cells was also able to suppress the endocytosis defect shown by the mutant. While Δ*ysl2* cells were strongly delayed in the turnover of Ste2p, in Δ*ysl2-ARL1* transformants the initial 45- to 47-kDa form of Ste2p disappeared rapidly upon addition of α-factor and the conversion to the hyperphosphorylated and ubiquitinylated form of Ste2p occurred more efficiently (Fig. 6B). However, this form of Ste2p persevered longer than in the wild type.

In addition to the partial restoration of Ste2p degradation, overproduction of Arl1p also suppressed the defect of vacuole fragmentation exhibited by Δ*ysl2* cells. A large fraction of Δ*ysl2-ARL1* transformants contained wild-type-like vacuoles, which accumulated LY after a 1-h incubation at 30°C (Fig. 6C).

To further establish a related function of Ysl2p and Arl1p, we tested for a synthetic genetic interaction between Δ*ysl2* and Δ*arl1* strains. A strain in which the majority of the *ARL1* gene was deleted was generated by replacing nucleotides 32 to 625 with the *URA3* gene cassette. As reported previously, Δ*arl1* cells grew similarly to wild-type cells under various conditions (28; B. Singer-Krüger, unpublished results). However, haploid progeny that were determined to harbor both Δ*ysl2* and Δ*arl1* were inviable, indicating a synthetic lethality (Fig. 6D). Together, these genetic data are highly indicative of a close functional relationship between Ys2p and Arl1p.

The N-terminal and putative Sec7 domains of Ysl2p mediate the binding to Arl1p. The presence of a putative Sec7 domain within Ysl2p and the genetic interaction between *YSL2* and *ARL1* suggested that Ysl2p may directly interact with Arl1p. This possibility was examined by the two-hybrid method. Reporter strain Y190 was cotransformed with various combinations of the *YSL2-SEC7* domain and *ARL1* plasmid constructs and the activity of β-galactosidase, a reporter enzyme of the two-hybrid system, was measured. We observed a weak but clearly measurable interaction of the Ysl2-Sec7 bait with wild-type Arl1p and two point mutants, $Arl1^{T32N}$ and $Arl1^{G30A}$, which, in analogy to Ras and other small GTPases, may keep Arl1p in either the GDP-bound or nucleotide-free form (Fig. 7A). However, a similar interaction was also measured for $Arl1^{Q72L}$, which has a mutation that corresponds to the dominant active mutation in Ras, the Ras^{Q61L} mutation, which was shown to keep Ras in the GTP-bound form (6). Very little interaction between the Ysl2 Sec7 domain and a $Ypt51^{S21N}$ fusion was observed. Although these results are indicative of an interaction between the Sec7 domains of Ysl2p and Arl1p, but not Ypt51p, it is unclear why the interaction was not dependent on the presumed nucleotide state of Arl1p. It was found that due to differences in the Arl1p crystal structure this small GTPase has a weaker affinity for Mg^{2+}, and therefore a stronger affinity for GDP, than most other Arf family members (2). Therefore, some fraction of the strongly overexpressed

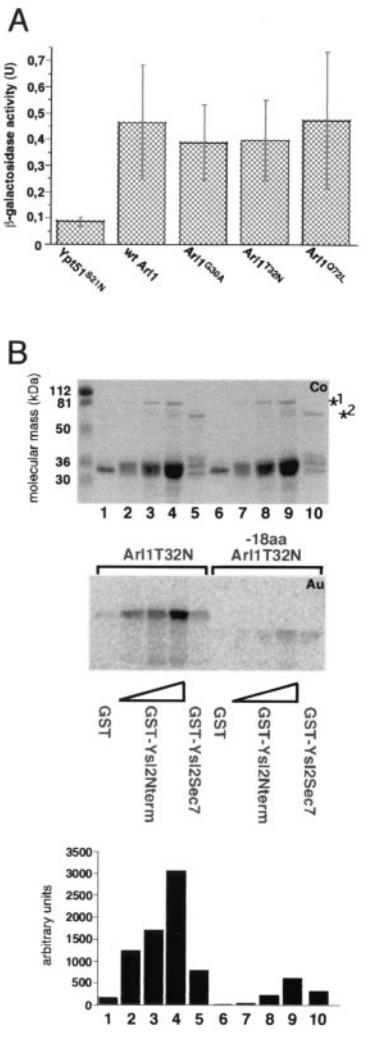

FIG. 7. Ysl2p binds to Arl1p via its Sec7 and N-terminal domains. (A) The Sec7 domain of Ysl2p interacts with Arl1p in the two-hybrid system. Strain Y190 was cotransformed with combinations of pAS1-Ysl2Sec7 and pACTII-Arl1wt, pACTII-18aaArl1^{T32N}, pACTII-18aaArl1^{G30A}, or pACTII-18aaArl1^{Q72L} and pACTII-Ysl2Sec7 and pAS1-Ypt51^{S21N}. Transformants were streaked out on SD-Leu, -Trp, and -His plates containing 25 mM 3-amino-1,2,4-triazole and analyzed for β-galactosidase activity as described in Materials and Methods. The values are the averages of three to five independent experiments with triplicate assays per transformant. Error bars, standard deviations. wt, wild type. (B) GST-Ysl2Sec7 and GST-Ysl2Nterm bind to in vitro-translated Arl1^{T32N}. Recombinant GST (10 μg; lane 1 and 6), GST-Ysl2Nterm (9.6, 19.2, and 38.4 μg in lanes 2 to 4 and 7 to 9, respectively), and GST-Ysl2Sec7 (30 μg; lanes 5 and 10) were purified from BL21 cells and immobilized onto glutathione-Sepharose beads. After incubation with ^{35}S-labeled in vitro-translated Arl1^{T32N} or −18aaArl1^{T32N}, the beads were washed and bound proteins were eluted by boiling them in SDS-PAGE sample buffer and separated by SDS-PAGE. Gels were either stained with Coomassie brilliant blue (Co) to reveal the GST fusions or processed for autoradiography (Au) to visualize Arl1^{T32N} and −18aaArl1^{T32N}. Quantitation of bound Arl1^{T32N} and −18aaArl1^{T32N} was performed with the phosphorimager. *1, full-length GST-Ysl2Nterm; *2, full-length GST-Ysl2Sec7.

Arl1 fusions may be bound to GDP in spite of the Q72L mutation and may interact with the Ysl2 Sec7 domain. Another possibility is that the Ysl2 Sec7 domain is not sufficient to distinguish between different nucleotide states of Arl1p.

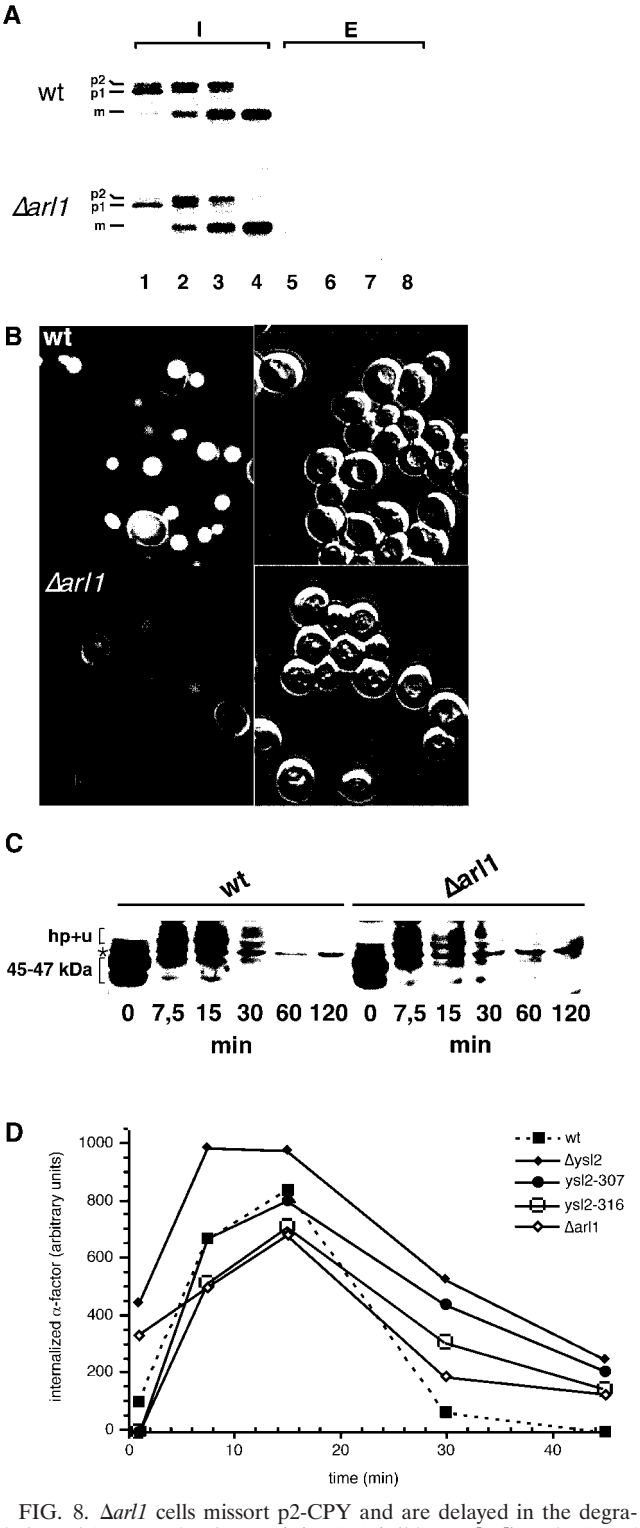

FIG. 8. Δ*arl1* cells missort p2-CPY and are delayed in the degradation of Ste2p and α-factor. (A) BS64 (wild type [wt]) and BS1005 (Δ*arl1*) cells were labeled for 5 min at 30°C with [^{35}S]methionine (lanes 1 and 5). Methionine was then added to initiate the chase for 5 (lanes 2 and 6), 10 (lanes 3 and 7), and 25 min (lanes 4 and 8). At each time point, aliquots of cells were removed and converted to spheroplasts after the medium (fraction E; lanes 5 to 8) was separated from the cells (fraction I; lanes 1 to 4). Fractions I and E were processed for immunoprecipitation with anti-CPY antibodies and analyzed by SDS-PAGE. p1, ER form; p2, Golgi form; m, mature form. (B) LY uptake in BS64 and BS1005 cells was monitored as described for Fig. 2B. Photographs were taken with identical exposure times by using fluorescence (left) and Nomarski optics (right). (C) Ste2p internalization assays were performed with BS64 and BS1005 cells at 30°C as described for Fig. 2A. *, band specifically labeled by the anti-Ste2p serum. (D) The degradation of intact and internalized ^{35}S-α-factor was quantified in strains BS64 (wild type), BS1005 (Δ*arl1*), BS694 (Δ*ysl2*), BS1023 (*ysl2-307*), and BS1024 (*ysl2-316*) as described in Materials and Methods subsequent to internalization periods of 1, 7.5, 15, 30, and 45 min at 30°C. After an initial increase in intact, internalized α-factor the data gave a linear decay curve on a logarithmic scale. The half-lives necessary to degrade 50% of the remaining intact α-factor were 4.2 (BS64), 10.7 (BS1005), 15.7 (BS694), 15 (BS1023), and 13.2 min (BS1024).

To confirm the two-hybrid interactions biochemically, we measured the binding of bacterially expressed recombinant GST-Ysl2p fusions to in vitro-translated Arl1p mutant proteins. For this purpose, two GST fusion proteins containing either amino acids 2 to 514 of Ysl2p (GST-Ysl2Nterm, including the Sec7 domain) or the Sec7 domain alone (GST-Ysl2Sec7, amino acids 211 to 514) were purified. The GST-Ysl2p fusion proteins or GST alone was immobilized on glutathione-Sepharose beads, and the binding of in vitro-translated full-length Arl1^{T32N} and −18aaArl1^{T32N}, lacking its 18 amino-terminal amino acids, was measured. Because both GST-Ysl2p fusions (Fig. 7B; Coomassie stained gel) were partially degraded, increasing amounts of GST-Ysl2Nterm were used in the binding assay to reach higher molar concentrations of undegraded GST fusions (Fig. 7B, lanes 2 to 4 and 7 to 9).

Consistent with the data from the two-hybrid system, −18aaArl1^{T32N} was found to be recruited by GST-Ysl2Sec7 (Fig. 7B, lane 10) and, to a twofold-greater degree, by GST-Ysl2Nterm (lane 9). No or very little binding of −18aaArl1^{T32N} or full-length Arl1^{T32N} to GST alone was found (lanes 6 and 1, respectively), even when GST was used at molar concentrations equivalent to those of the potential GST-Ysl2p breakdown products in lanes 4 and 9. Upon addition of a quantity of full-length Arl1^{T32N} similar to the quantity of added −18aaArl1^{T32N}, a striking increase in the binding, in particular to GST-Ysl2Nterm, was observed (compare lanes 2 to 4 with lanes 7 to 9). The recruitment of Arl1^{T32N} by GST-Ysl2Nterm occurred in a concentration-dependent manner. Again, full-length Arl1^{T32N} was found to bind more efficiently to GST-Ysl2Nterm than to GST-Ysl2Sec7 (compare lanes 2 to 4 with 5), even at low concentrations of GST-Ysl2Nterm (lane 2). Therefore, even though the Sec7 domain of Ysl2p appeared to be sufficient for binding to Arl1p, the additional presence of the N-terminal domain of Ysl2p strongly enhanced the binding to Arl1p. Moreover, it can be concluded that the N-terminal helix of Arl1p, which is involved in myristylation (28) and which may interact with membranes and effectors, strongly facilitated the binding to Ysl2p. The observed interaction between Arl1p and Ysl2p was most likely direct, unless the reticulocyte lysate contained a conserved molecule that could substitute for the corresponding yeast homolog during complex formation between Ysl2p and Arl1p.

Arl1p is required for endocytosis and biosynthetic sorting of CPY to the vacuole. The fact that *ARL1* interacted with *YSL2* suggested that, similar to Ysl2p, the small GTPase may function in endocytosis and vacuole biogenesis. In a recent study,

the Δ*arl1* null mutant was reported to exhibit no defect in ER-to-Golgi and intra-Golgi transport (28). Therefore, we characterized the Δ*arl1* deletion strain with respect to trafficking within the endosomal system. Δ*arl1* cells cosegregated with a release of CPY to the extracellular medium (data not shown). To determine whether this was due to missorting via the secretory pathway, pulse-chase labeling with [^{35}S]methionine and immunoprecipitation were performed to monitor the biogenesis and sorting of CPY. In Δ*arl1* cells, CPY was processed with kinetics that were similar to those of the wild type (Fig. 8A). However, a small but clearly detectable fraction of Golgi-modified p2CPY was missorted to the extracellular medium (11% of total CPY). This fraction of secreted CPY was similar to that missorted by Δ*ysl2* cells.

Although the morphology of Δ*arl1* vacuoles appeared similar to that of wild-type vacuoles, upon endocytosis of fluid phase marker LY, mutant vacuoles accumulated less dye than those of the wild type (Fig. 8B). To determine whether the endocytic delivery of a plasma membrane receptor to the vacuole may also be defective, we monitored the turnover of Ste2p. As shown in Fig. 8C, we found that the ligand-induced degradation of Ste2p was delayed in the Δ*arl1* mutant compared to that for the wild type. The time necessary to fully degrade the intact 45- to 47-kDa form of Ste2p increased to more than 120 min in the Δ*arl1* mutant, while in the wild type after 60 min this band was absent, and the degradation of the hyperphosphorylated and polyubiquitinylated form was also delayed (Fig. 8C). A quantitative analysis of the time necessary to degrade internalized ^{35}S-labeled α-factor in Δ*arl1* cells compared to that for the wild type and *ysl2* mutants also confirmed that deletion of *ARL1* caused a delay in endocytic pheromone turnover (Fig. 8D). In comparison to the times for Δ*ysl2*, *ysl2-307*, or *ysl2-316* strains, the delay was, however, less striking (Fig. 8D). Together, these results corroborate the LY data and suggest a function for Arl1p in trafficking within the endosomal system.

DISCUSSION

Ysl2p reveals structural homology to high-molecular-weight Arf GEFs. In this study we characterize a novel yeast protein, Ysl2p, which reveals significant sequence homology to the Sec7 family of Arf GEFs. Members of this family form two major classes. While the smaller (<100 kDa) Sec7 GEFs, including for example ARNO, cytohesin-1, and EFA6, have to date only been identified in higher eukaryotes, the larger Sec7 family members (>100 kDa) have orthologs in all eukaryotes examined and are therefore suggested to play highly conserved roles in membrane dynamics (22). Four Sec7 domain proteins of this class in *Saccharomyces cerevisiae* were previously described: Sec7p (12), Gea1p, Gea2p (38), and Syt1p, the last one being the most distant relative (23). The studies presented here, provided three lines of in silico evidence to support the idea that Ysl2p represents yet another high-molecular-weight Sec7 family member. First, multiple sequence alignment of the 284-amino-acid putative Sec7 domain of Ysl2p with 24 other Sec7 domains revealed a remote but significant homology to this domain. Second, secondary structure prediction analysis predicted the existence of 10 α-helices within the putative Sec7 domain of Ysl2p, identical with the number of α-helices found in the crystal structure of the ARNO Sec7 domain. Thus, in spite of the remote sequence identity (i.e., the absence of a conserved glutamate located at position 156 in the ARNO Sec7 domain [4]), the underlying structural propensity of this domain is highly similar to those of other Sec7 domains. Finally, the homology to Sec7 family members was not restricted to the Sec7 domain but was also apparent within the region located amino terminally to it. Even though the function of this novel highly conserved N-terminal domain of Ysl2p (amino acids 1 to 175) and other Sec7 GEFs such as BIG1 and BIG2 is unknown, our biochemical data (see below) suggest that it may also be implicated in the formation of complexes with Arf/Arl family members.

Ysl2p reveals functional homology to Sec7 family members. Our genetic and biochemical data clearly suggested that Ysl2p interacts with the Arf family member Arl1p. The defect of the Δ*ysl2* strain in growth, endocytosis, and vacuole biogenesis could be suppressed specifically by the overexpression of Arl1p, but not that of other Arl proteins, and Δ*ysl2* Δ*arl1* double mutants displayed synthetic lethality at 25°C, which is permissive for growth of the single mutants. Evidence in support of a direct interaction between Ysl2p and Arl1p was provided by the two-hybrid system and an in vitro binding assay. While the presence of the Sec7 domain was sufficient to detect a weak interaction with Arl1p, the additional presence of the N-terminal domain of Ysl2p significantly enhanced the binding to Arl1p, in particular to the full-length protein. Since the N-terminal domain is a second sequence element of Ysl2p with homology to large Sec7 GEFs such as BIG1 and BIG2, the enhanced binding implies that this region may generally be important for the interaction of related Sec7 family members with Arf/Arl small GTPases. Interestingly, the interaction between Ysl2p and Arl1p was also highly sensitive to the presence of the amino terminus of Arl1p. This domain of Arf/Arl family members is a nucleotide-sensitive region with a covalently attached myristate which acts as a "myristoyl switch" to coordinate activation (GTP binding) with translocation onto a membrane (5). In fact, the recent structural resolution of Arl1p (2) and the finding that Arl1p is myristylated (28) indicate that the amino terminus of Arl1p is structurally similar to that of other Arf family members and therefore may also act as a myristoyl switch. Our finding that it enhances the formation of a complex with Ysl2p is also be in agreement with evidence suggesting that the amino terminus of Arf family members may influence the binding to effectors which can increase the stoichiometry of the binding of GTP to Arf proteins (25, 60).

Even though evidence for nucleotide exchange activity, most likely toward Arl1p, has still to be provided, additional hints support the notion that Ysl2p could be involved in such an activity. First, systematic analysis of all *S. cerevisiae* deletion mutants for drug sensitivity has revealed that Δ*ysl2* cells exhibit an increased sensitivity for the drug BFA, a fungal toxin that acts as an uncompetitive inhibitor stabilizing an Arf-GDP-Sec7-GEF protein complex (39). The increased BFA sensitivity of Δ*ysl2* cells would be consistent with the idea that, like the other yeast Sec7 family members, Ysl2p represents a target for BFA (23, 39). Second, Δ*ysl2* cells and cells carrying the temperature-sensitive alleles *ysl2-307* and *ysl2-316* reveal highly fragmented vacuoles. The drastic breakdown of the vacuolar compartment that occurred immediately upon inactivation of

Ysl2p is reminiscent of the loss of organelle identity, in particular of the Golgi, immediately observed after BFA treatment (27). Thus, an intriguing explanation for the loss of vacuole integrity upon temperature inactivation of Ysl2p could be the inhibition of an activity that resembles Arf-GEF. There could be multiple reasons for the apparent absence of nucleotide dependence in the two-hybrid interaction between the Ysl2 Sec7 domain and Arl1p. One possibility is that the Sec7 domain of Ysl2p may not be sufficient to distinguish between different nucleotide states of Arl1p. This would be consistent with the observation that the genetic interaction between full-length *YSL2* and *ARL1* was dependent on the nucleotide state of Arl1p (B. Singer-Krüger, unpublished observation).

Ysl2p has a direct function in endocytosis and in the maintenance of vacuole integrity. In this study we show that Ysl2p is required for the endocytic transport of Ste2p and α-factor to the vacuole, where degradation occurs. The Δ*ysl2* strain exhibited almost no ligand-induced degradation of Ste2p and a strongly reduced rate of α-factor degradation. Furthermore, the temperature-sensitive *ysl2-307* and *ysl2-316* mutants were clearly defective in the turnover of Ste2p and α-factor even at their permissive growth temperature. At this temperature, secretory functions such as the processing of CPY and the secretion of invertase were unimpaired and the vacuolar sorting of CPY was only marginally affected. The block in Ste2p turnover appeared more pronounced in Δ*ysl2* mutants than in the temperature-sensitive *ysl2* mutants, while α-factor degradation was delayed similarly in these strains. Since ubiquitinylation of Ste2p, which plays an important role in sorting within the endosomal/vacuolar compartment, appeared to be more reduced in Δ*ysl2* than in the *ysl2* temperature-sensitive mutants, it is possible that this could explain the more extensive stabilization of membrane-bound Ste2p. Consistent with a localization of Ysl2p on endosomal elements, the Ysl2p staining was sensitive to a mutation in *VPS27* but not in *SEC7*. In addition, GFP-tagged Ysl2p colocalized with endocytosed FM4-64. Collectively, these data strongly support a major role for Ysl2p in endocytic trafficking.

Using several experimental strategies, we also show that Ysl2p has a function in the process that controls the structural maintenance of the vacuolar compartment. In vivo studies using the temperature-sensitive *ysl2-307* and *ysl2-316* mutants demonstrated that fragmentation, evident both by light and electron microscopy, is an immediate and thus most likely a direct consequence of inactivation of Ysl2p. Consistent with that, an in vitro assay that measures homotypic fusion between vacuoles (17) revealed a strong deficiency in the fusogenic activity of Δ*ysl2* vacuoles (A. Jochum and B. Singer-Krüger, unpublished results). In support of the idea that Ysl2p and Arl1p collaborate in a common process, a partial restoration of vacuole fusion could be observed both in vivo and in vitro upon the overexpression of Arl1p in the Δ*ysl2* strain. However, since Ysl2p was not detected on vacuoles by subcellular fractionation (Fig. 4A) (S. Wicky and B. Singer-Krüger, unpublished results) and microscopy (Fig. 5), it may not be a component of the fusion machinery and therefore may not be directly required for the fusion reaction. Rather, it is conceivable that Ysl2p is necessary to provide components that are directly involved in the fusion reaction.

Consistent with our data that revealed an interaction between Ysl2p and Arl1p, it appears that Arl1p also functions in endocytosis and vacuolar protein sorting. Therefore, our work provides the first evidence for the implication of an Arl family member in the process of endocytosis.

Ysl2p displays a genetic interaction with Δ*ypt51* cells. Originally, *ysl2-1* was identified due to its synthetic lethality with the Δ*ypt51* strain (49). Consistent with that, similar genetic interactions between genes encoding several other Arf GEFs and Rab/Ypt family members have been observed (23). Since members of the Sec7 family were not found to act as GEFs for the Ypt GTPases, it was suggested that Arf and Ypt GTPases may interact in a regulatory cascade (23) similar, for example, to the one in which the small GTPases Bud1p and Cdc42p are linked via the Cdc42p GEF, Cdc24p, to control bud formation (59). Our findings lend further support of Ypt-Arf GTPase cascades, in which, for example, Arl1p and/or other Arf family members and endocytic Ypts may be linked through the action of accessory proteins, such as Ysl2p, to regulate endocytosis and vacuole biogenesis. The challenge now is to determine the mechanism by which Arfs, Ypts, and GEFs interact to regulate different aspects of endocytosis and vacuole biogenesis.

ACKNOWLEDGMENTS

We are very grateful to Cathy Jackson, Howard Riezman, Kathleen D'Hondt, Xin Nie, and Steve Elledge for providing plasmids and reagents used in this study. We acknowledge Sabine Frischmuth for assistance in the screen for temperature-sensitive mutants of *ysl2*, Evi Frei for help in the purification of ^{35}S-labeled α-factor, Yvonne Volkenstein for technical assistance, and Dieter H. Wolf for critical reading of the manuscript.

This work was supported by a grant from the DFG to B.S.-K. (Si 635/2-1).

REFERENCES

1. **Altschul, S. F., T. L. Madden, A. A. Schaffer, J. Zhang, Z. Zhang, W. Miller, and D. J. Lipman.** 1997. Gapped BLAST and PSI-BLAST: a new generation of protein database search programs. Nucleic Acids Res. **25:**3389–3402.
2. **Amor, J. C., J. R. Horton, X. Zhu, Y. Wang, C. Sullards, D. Ringe, X. Cheng, and R. A. Kahn.** 2001. Structures of yeast ARF2 and ARL1. J. Biol. Chem. **276:**42477–42484.
3. **Barik, S., and M. Galinski.** 1991. "Megaprimer"method of PCR: increased template concentration improves yield. BioTechniques **10:**489–490.
4. **Beraud-Dufour, S., S. Robineau, P. Chardin, S. Paris, M. Chabre, J. Cherfils, and B. Antonny.** 1998. A glutamic finger in the guanine nucleotide exchange factor ARNO displaces Mg^{2+} and the beta-phosphate to destabilize GDP on ARF1. EMBO J. **17:**3651–3659.
5. **Beraud-Dufour, S., and W. E. Balch.** 2001. Structural and functional organization of ADP-ribosylation factor (ARF) proteins. Methods Enzymol. **329:**245–247.
6. **Bourne, H. R., D. A. Sanders, and F. McCormick.** 1991. The GTPase superfamily: conserved structure and molecular mechanism. Nature **349:**117–127.
7. **Chardin, P., S. Paris, B. Antonny, S. Robineau, S. Beraud-Dufour, C. L. Jackson, and M. Chabre.** 1996. A human exchange factor for ARF contains Sec7- and pleckstrin-homology domains. Nature **384:**481–484.
8. **Cherfils, J., J. Menetrey, M. Mathieu, G. Le Bras, S. Robineau, S. Beraud-Dufour, and B. Antonny.** 1998. Structure of the Sec7 domain of the Arf exchange factor ARNO. Nature **392:**101–105.
9. **Claros, M. G., and G. von Heijne.** 1994. TopPred II: an improved software for membrane protein structure predictions. Comput. Appl. Biosci. **10:**685–686.
10. **Dulic, V., M. Egerton, I. Elguindi, S. Raths, B. Singer, and H. Riezman.** 1991. Yeast endocytosis assays. Methods Enzymol. **194:**679–710.
11. **Eddy, S. R.** 1996. Hidden Markov models. Curr. Opin. Struct. Biol. **6:**361–365.
12. **Franzusoff, A., and R. Schekman.** 1989. Functional compartments of the yeast Golgi apparatus are defined by the *sec7* mutation. EMBO J. **8:**2695–2702.
13. **Gaynor, E. C., C. Y. Chen, S. D. Emr, and T. R. Graham.** 1998. ARF is required for maintenance of yeast Golgi and endosome structure and function. Mol. Biol. Cell **9:**653–670.
14. **Gerrard, S. R., N. J. Bryant, and T. H. Stevens.** 2000. *VPS21* controls entry

of endocytosed and biosynthetic proteins into the yeast prevacuolar compartment. Mol. Biol. Cell **11:**613–626.
15. **Goldstein, A., and J. O. Lampen.** 1975. Beta-D-fructofuranoside fructohydolase from yeast. Methods Enzymol. **42:**504–511.
16. **Guarente,L.** 1983. Yeast promoters and lacZ fusions designed to study expression of cloned genes in yeast. Methods Enzymol. **101:**181–191.
17. **Haas, A., B. Conradt, and W. Wickner.** 1994. G-protein ligands inhibit in vitro reactions of vacuole inheritance. J. Cell Biol. **126:**87–97.
18. **Hicke, L., and H. Riezman.** 1996. Ubiquitination of a yeast plasma membrane receptor signals its ligand-stimulated endocytosis. Cell **84:**277–287.
19. **Hillig, R. C., M. Hanzal-Bayer, M. Linari, J. Becker, A. Wittinghofer, and L. Renault.** 2000. Structural and biochemical properties show ARL3-GDP as a distinct GTP binding protein. Struct. Fold. Des. **8:**1239–1245.
20. **Hohenberg, H., K. Mannweiler, and M. Müller.** 1994. High-pressure freezing of cell suspensions in cellulose capillary tubes. J. Microsc. **175:**34–43.
21. **Horazdovsky, B. F., G. Busch, and S. D. Emr.** 1994. *VPS21* encodes a rab5-like GTP binding protein that is required for the sorting of yeast vacuolar proteins. EMBO J. **13:**1297–1309.
22. **Jackson, C. L., and J. E. Casanova.** 2000. Turning on ARF: the Sec7 family of guanine-nucleotide-exchange factors. Trends Cell Biol. **10:**60–67.
23. **Jones, S., G. Jedd, R. A. Kahn, A. Franzusoff, F. Bartolini, and N. Segev.** 1999. Genetic interactions in yeast between Ypt GTPases and Arf guanine nucleotide exchangers. Genetics **152:**1543–1556.
24. **Kahn, R. A., and A. G. Gilman.** 1984. ADP-ribosylation of Gs promotes the dissociation of its alpha and beta subunits. J. Biol. Chem. **259:**6235–6240.
25. **Kahn, R. A., P. Randazzo, T. Serafini, O. Weiss, C. Rulka, J. Clark, M. Amherdt, P. Roller, L. Orci, and J. E. Rothman.** 1992. J. Biol. Chem. **267:**13039–13046.
26. **Kahn, R. A.** 1995. The Arf subfamily. Oxford University Press, Oxford, United Kingdom.
27. **Klausner, R. D., J. G. Donaldson, and J. Lippincott-Schwartz.** 1992. Brefeldin A: insights into the control of membrane traffic and organelle structure. J. Cell Biol. **116:**1071–1080.
28. **Lee, F. J. S., C. F. Huang, W. L. Yu, L. M. Buu, C. Y. Lin, M. C. Huang, J. Moss, and M. Vaughan.** 1997. Characterization of an ADP-ribosylation factor-like 1 protein in *Saccharomyces cerevisiae*. J. Biol. Chem. **272:**30998–31005.
29. **Letourneur, F., E. C. Gaynor, S. Hennecke, C. Demolliere, R. Duden, S. D. Emr, H. Riezman, and P. Cosson.** 1994. Coatomer is essential for retrieval of dilysine-tagged proteins to the endoplasmic reticulum. Cell **79:**1199–1207.
30. **Longtine, M. S., A. McKenzie, D. J. Demarini, N. G. Shah, A. Wach, A. Brachat, P. Philippsen, and J. R. Pringle.** 1998. Additional modules for versatile and economical PCR-based gene deletion and modification in *Saccharomyces cerevisiae*. Yeast **14:**953–961.
31. **Mansour, S. J., J. Skaug, X. H. Zhao, J. Giordano, S. Scherer, and P. Melancon.** 1999. p200 ARF-GEP1: a Golgi-localized guanine nucleotide exchange protein whose Sec7 domain is targeted by the drug brefeldin A. Proc. Natl. Acad. Sci. USA **96:**7968–7973.
32. **McGuffin, L. J., K. Bryson, and D. T. Jones.** 2000. The PSIPRED protein structure prediction server. Bioinformatics **16:**404–405.
33. **Morinaga, N., R. Adamik, J. Moss, and M. Vaughan.** 1999. Brefeldin A inhibited activity of the Sec7 domain of p200, a mammalian guanine nucleotide-exchange protein for ADP-ribosylation factors. J. Biol. Chem. **274:**17417–17423.
34. **Moss, J., and M. Vaughan.** 1998. Molecules in the ARF orbit. J. Biol. Chem. **273:**21431–21434.
35. **Mossessova, E., J. M. Gulbis, and J. Goldberg.** 1998. Structure of the guanine nucleotide exchange factor of the Sec7 domain of human Arno and analysis of the interaction with ARF GTPase. Cell **92:**415–423.
36. **Muhlrad, D., R. Hunter, and R. Parker.** 1992. A rapid method for localized mutagenesis of yeast genes. Yeast **8:**79–82.
37. **Novick, P., S. Ferro, and R. Schekman.** 1981. Order of events in the yeast secretory pathway. Cell **25:**461–469.
38. **Peyroche, A., S. Paris, and C. L. Jackson.** 1996. Nucleotide exchange on ARF mediated by yeast Geal protein. Nature **384:**479–481.
39. **Peyroche, A., B. Antonny, S. Robineau, J. Acker, J. Cherfils, and C. L. Jackson.** 1999. Brefeldin A acts to stabilize an abortive ARF-GDP-Sec7 domain protein complex: involvement of specific residues of the Sec7 domain. Mol. Cell **3:**275–285.
40. **Piper, R. C., A. A. Cooper, H. Yang, and T. H. Stevens.** 1995. VPS27 controls vacuolar and endocytic traffic through a prevacuolar compartment in *Saccharomyces cerevisiae*. J. Cell Biol. **131:**603–617.
41. **Prescianotto-Baschong, C., and H. Riezman.** 2002. Ordering of compartments in the yeast endocytic pathway. Traffic **3:**37–49.
42. **Rost, B., P. Fariselli, and R. Casadio.** 1996. Topology prediction for helical transmembrane proteins at 86% accuracy. Protein Sci. **5:**1704–1718.
43. **Schandel, K. A., and D. D. Jenness.** 1994. Direct evidence for ligand-induced internalization of the yeast a-factor pheromone receptor. Mol. Cell. Biol. **14:**7245–7255.
44. **Schultz, J., R. R. Copley, T. Doerks, C. P. Ponting, and P. Bork.** 2000. SMART: a web-based tool for the study of genetically mobile domains. Nucleic Acids Res. **28:**231–234.
45. **Sharer, J. D., and R. A. Kahn.** 1999. The ARF-like 2 (ARL2)-binding protein, BART. Purification, cloning, and initial characterization. J. Biol. Chem. **274:**27553–27561.
46. **Singer-Krüger, B., R. Frank, F. Crausaz, and H. Riezman.** 1993. Partial purification and characterization of early and late endosomes from yeast. J. Biol. Chem. **268:**14376–14386.
47. **Singer-Krüger, B., H. Stenmark, A. Düsterhöft, P. Philippsen, J.-S. Yoo, D. Gallwitz, and M. Zerial.** 1994. Role of three rab5-like GTPases, Ypt51p, Ypt52p, and Ypt53p, in the endocytic and vacuolar protein sorting pathways of yeast. J. Cell Biol. **125:**283–298.
48. **Singer-Krüger, B., H. Stenmark, and M. Zerial.** 1995. Yeast Ypt51p and mammalian Rab5: counterparts with similar function in the early endocytic pathway. J. Cell Sci. **108:**3509–3521.
49. **Singer-Krüger, B., and S. Ferro-Novick.** 1997. Use of a synthetic lethal screen to identify yeast mutants impaired in endocytosis, vacuolar protein sorting and the organization of the cytoskeleton. Eur. J. Cell Biol. **74:**365–375.
50. **Sonnhammer, E. L., G. von Heijne, and A. Krogh.** 1998. A hidden Markov model for predicting transmembrane helices in protein sequences. Proc. Int. Conf. Intell. Syst. Mol. Biol. **6:**175–182.
51. **Stearns, T., R. A. Kahn, D. Botstein, and M. A. Hoyt.** 1990. ADP ribosylation factor is an essential protein in *Saccharomyces cerevisiae* and is encoded by two genes. Mol. Cell. Biol. **10:**6690–6699.
52. **Thompson, J. D., D. G. Higgins, and T. J. Gibson.** 1994. CLUSTAL W: improving the sensitivity of progressive multiple sequence alignment through sequence weighting, position-specific gap penalties and weight matrix choice. Nucleic Acids Res. **22:**4673–4680.
53. **Togawa, A., N. Morinaga, M. Ogasawara, J. Moss, and M. Vaughan.** 1999. Purification and cloning of a brefeldin A-inhibited guanine nucleotide-exchange protein for ADP-ribosylation factors. J. Biol. Chem. **274:**12308–12315.
54. **Van Valkenburgh, H., J. F. Shern, J. D. Sharer, X. Zhu, and R. A. Kahn.** 2001. ADP-ribosylation factors (ARFs) and ARF-like 1 (ARL1) have both specific and shared effectors: characterizing ARL1 binding proteins. J. Biol. Chem. **276:**22826–22837.
55. **Vida, T. A., and S. D. Emr.** 1995. A new vital stain for visualizing vacuolar membrane dynamics and endocytosis in yeast. J. Cell Biol. **128:**779–792.
56. **Wach, A., A. Brachat, R. Pohlmann, and P. Philippsen.** 1994. New heterologous modules for classical or PCR-based gene disruptions in *Saccharomyces cerevisiae*. Yeast **10:**1793–1808.
57. **Yahara, N., T. Ueda, K. Sato, and A. Nakano.** 2001. Multiple roles of Arf1 GTPase in the yeast exocytic and endocytic pathways. Mol. Biol. Cell **12:**221–238.
58. **Zerial, M., and H. McBride.** 2001. Rab proteins as membrane organizers. Nat. Rev. Mol. Cell Biol. **2:**107–117.
59. **Zheng, Y., A. Bender, and R. A. Cerione.** 1995. Interactions among proteins involved in bud-site selection and bud-site assembly in *Saccharomyces cerevisiae*. J. Biol. Chem. **270:**626–630.
60. **Zhu, X., A. L. Boman, J. Kuai, W. Cieplak, and R. A. Kahn.** 2000. Effectors increase the affinity of ADP-ribosylation factor for GTP to increase binding. J. Biol. Chem. **275:**13465–13475.